PERGAMON

Journal of Structural Geology 25 (2003) 717–736

JOURNAL OF STRUCTURAL GEOLOGY

www.elsevier.com/locate/jstrugeo

Geochemistry, mineralization, structure, and permeability of a normal-fault zone, Casino mine, Alligator Ridge district, north central Nevada

K. Jill Hammond[1], James P. Evans*

Department of Geology, Utah State University, 4505 Old Main Hill, Logan, UT 84322-4505, USA

Received 2 May 2001; accepted 1 May 2002

Abstract

We examine the geochemical signature and structure of the Keno fault zone to test its impact on the flow of ore-mineralizing fluids, and use the mined exposures to evaluate structures and processes associated with normal fault development. The fault is a moderately dipping normal-fault zone in siltstone and silty limestone with 55–100 m of dip-slip displacement in north-central Nevada. Across-strike exposures up to 180 m long, 65 m of down-dip exposure and 350 m of along-strike exposure allow us to determine how faults, fractures, and fluids interact within mixed-lithology carbonate-dominated sedimentary rocks. The fault changes character along strike from a single clay-rich slip plane 10–20 mm thick at the northern exposure to numerous hydrocarbon-bearing, calcite-filled, nearly vertical slip planes in a zone 15 m wide at the southern exposure. The hanging wall and footwall are intensely fractured but fracture densities do not vary markedly with distance from the fault. Fault slip varies from pure dip-slip to nearly pure strike-slip, which suggests that either slip orientations may vary on faults in single slip events, or stress variations over the history of the fault caused slip vector variations. Whole-rock major, minor, and trace element analyses indicate that Au, Sb, and As are in general associated with the fault zone, suggesting that Au- and silica-bearing fluids migrated along the fault to replace carbonate in the footwall and adjacent hanging wall rocks. Subsequent fault slip was associated with barite and calcite and hydrocarbon-bearing fluids deposited at the southern end of the fault. No correlation exists at the meter or tens of meter scale between mineralization patterns and fracture density.

We suggest that the fault was a combined conduit-barrier system in which the fault provides a critical connection between the fluid sources and fractures that formed before and during faulting. During the waning stages of deposit formation, the fault behaved as a localized conduit to hydrocarbon-bearing calcite veins. The results of this study show that fault-zone character may change dramatically over short, deposit- or reservoir-scale distances. The presence of damage zones may not be well correlated at the fine scale with geochemically defined regions of the fault, even though a gross spatial correlation may exist.

Keywords: Fault; Ore deposits; Fluid-flow; Disseminated gold; Carlin

1. Introduction

Faults and related fractures play an important role in fluid migration throughout the upper crust (e.g. Sibson and Scott, 1998). Often, however, the relationship between a fault zone, its hydraulic properties, and the hydrogeologic setting during fault slip and fluid flow is poorly understood. To better understand the association between structures and fluid migration, it is important to examine the architecture and petrology of faults, which helps to determine if and how fluids flow through a fault zone.

The hydrology and structure of fault zones can be divided into three components: the fault core (which accommodates slip and is often accompanied by low permeability gouge or mineral precipitates), the damage zone (fractured footwall and hanging wall rocks), and undeformed protolith (Chester and Logan, 1986; Smith et al., 1990; Caine et al., 1996). The amount and distribution of each of these components determine the fault-zone architecture and the permeability structure of a fault zone (Caine et al., 1996; Sigda et al., 1999; Rawling et al., 2001). Studies in clastic rocks (Chester and Logan, 1986), carbonate rocks (Hanks et al., 1997; Mollema and Antonellini, 1999), igneous rocks (Bruhn et al., 1994; Seront et al., 1998; Escuder Viruete et al., 2001), metamorphic rocks (Chester et al., 1993; Schulz and Evans, 1998), and poorly consolidated sediments (Heynekamp et al., 1999) show that higher fracture densities are often

* Corresponding author. Fax: +801-797-1588.
E-mail address: jpevans@cc.usu.edu (J.P. Evans).
[1] Now at: ExxonMobil Exploration Company, 233 Benmar, Houston, TX 77060, USA.

0191-8141/03/$ - see front matter © 2002 Elsevier Science Ltd. All rights reserved.
PII: S0191-8141(02)00060-3

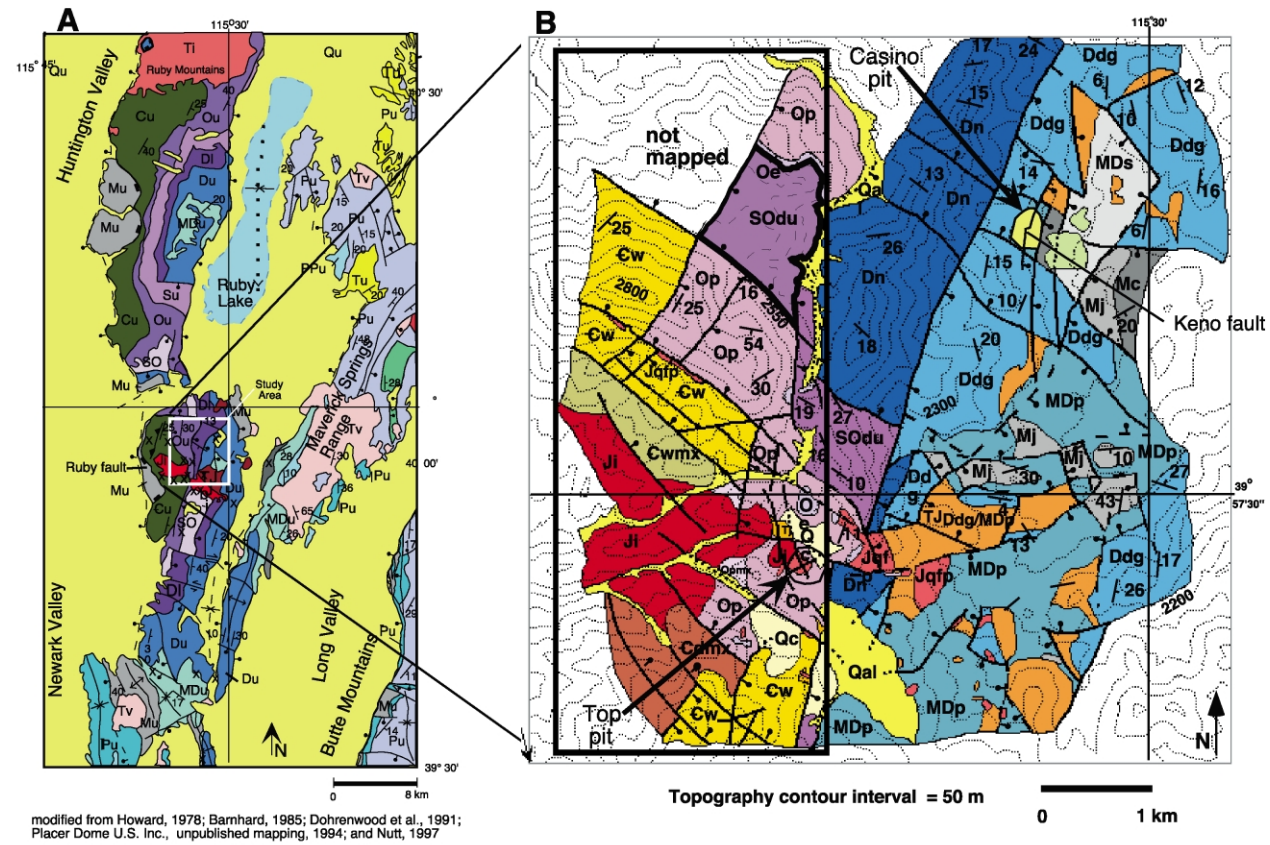
A
B
Huntington Valley
Ruby Mountains
Ruby Lake
Ruby fault
Study Area
Maverick Springs Range
Newark Valley
Long Valley
Butte Mountains
Casino pit
Top pit
not mapped
Keno fault
Topography contour interval = 50 m
0 1 km
modified from Howard, 1978; Barnhard, 1985; Dohrenwood et al., 1991; Placer Dome U.S. Inc., unpublished mapping, 1994; and Nutt, 1997

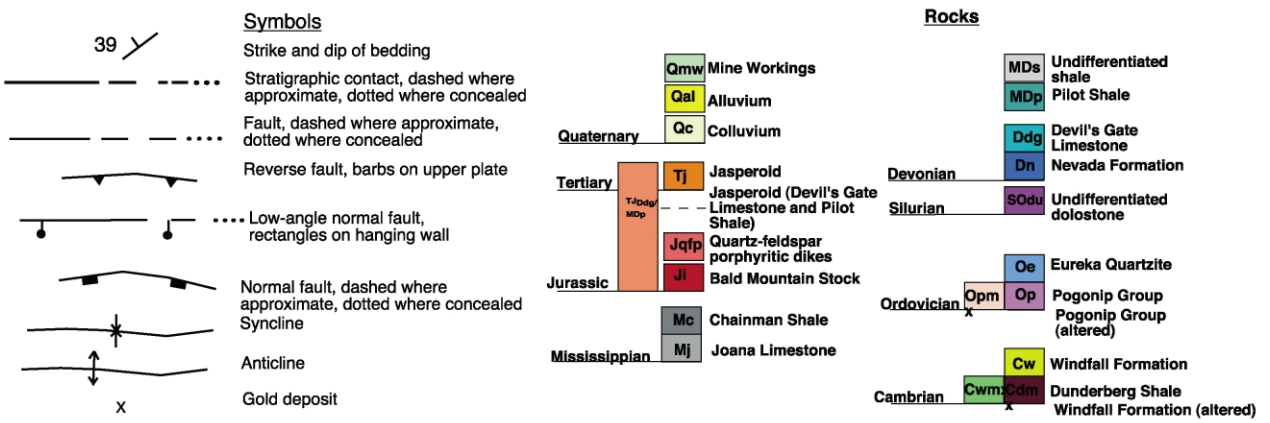
Symbols
Strike and dip of bedding
Stratigraphic contact, dashed where approximate, dotted where concealed
Fault, dashed where approximate, dotted where concealed
Reverse fault, barbs on upper plate
Low-angle normal fault, rectangles on hanging wall
Normal fault, dashed where approximate, dotted where concealed
Syncline
Anticline
Gold deposit
Rocks
Mine Workings
Alluvium
Colluvium
Quaternary
Tertiary
Jurassic
Jasperoid
Jasperoid (Devil's Gate Limestone and Pilot Shale)
Quartz-feldspar porphyritic dikes
Bald Mountain Stock
Mississippian
Chainman Shale
Joana Limestone
Undifferentiated shale
Pilot Shale
Devil's Gate Limestone
Devonian
Nevada Formation
Silurian
Undifferentiated dolostone
Eureka Quartzite
Ordovician
Pogonip Group
Pogonip Group (altered)
Windfall Formation
Cambrian
Dunderberg Shale
Windfall Formation (altered)

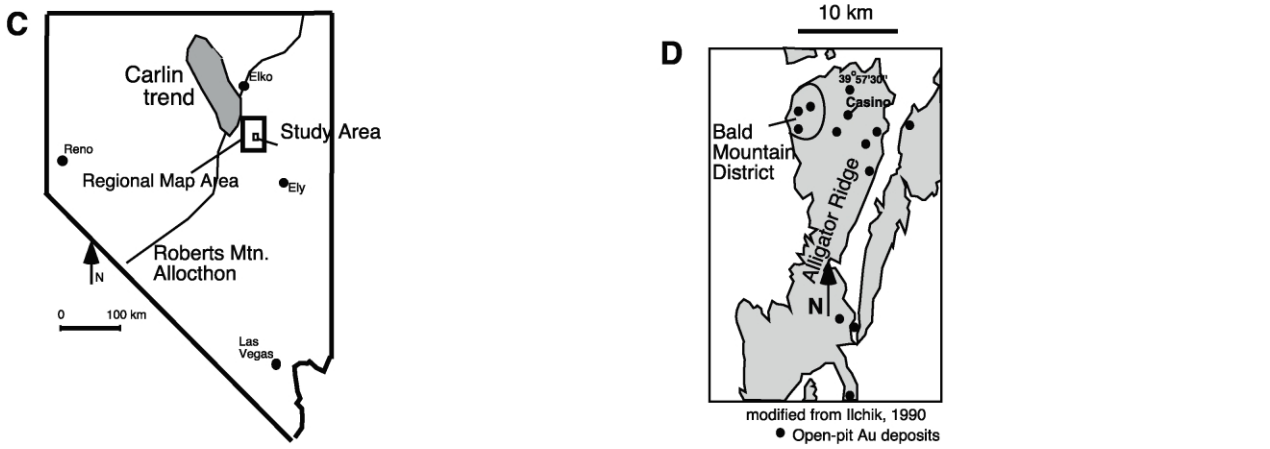
C
Carlin trend
Elko
Study Area
Reno
Regional Map Area
Ely
Roberts Mtn. Allocthon
Las Vegas
0 100 km
D
10 km
Bald Mountain District
Alligator Ridge
Casino
modified from Ilchik, 1990
Open-pit Au deposits

spatially related to faults and that fractures are the main deformational components within damage zones (Caine et al., 1996; Schulz and Evans, 1998). Within fault zones, fluid flow may be concentrated along these fractures (Schulz et al., 1998; Seront et al., 1998; Sibson and Scott, 1998). In some cases permeabilities of the fractured damage zone are several orders of magnitude greater than that of the fault core or protolith (Evans et al., 1997; Seront et al., 1998; Caine and Forster, 1999). Chester and Logan (1986) found that as the fracture intensity in the damage zone increased toward the main slip surface in sedimentary rocks, permeability increased from protolith towards the gouge. However, the permeability of gouge is significantly lower than that of the surrounding rock (Chester and Logan, 1986).

Common techniques for collecting fault and fracture data include linear transect (1-D) and box (2-D) methods (e.g. Titley et al., 1986; Gillespie et al., 1993; Schulz and Evans, 1998; Caine and Forster, 1999), in which fault zone thickness, petrology, geometry, and orientation of the fault core, and distance of fractures from the fault core, their length, connectivity, aperture, mineral filling/coating (Caine and Forster, 1999) are recorded. To quantify the permeability of a fault zone, permeability tests may be conducted (e.g. Chester and Logan, 1986; Evans et al., 1997) or fluid-flow simulation models may be constructed (e.g. Caine and Forster, 1999; Committee on Fracture Characterization and Fluid Flow, 1996). Qualitative methods involve determining the ratio of fault-zone-architecture elements (Caine et al., 1996) as described above or conducting a geochemical study to determine the distribution of fluid-flow indicators (e.g. Schulz and Evans, 1998) such as economic minerals, hydrocarbons, silica, or calcite.

While the previous studies listed above shed light on faults that cut rocks with relatively high strength, little work has examined fault zones in weaker rocks with high clay or silt components (with the notable exceptions of Heynekamp et al. (1999) and Sigda et al. (1999)), nor over length scales of 10–300 m. Such faults are important for the migration of hydrocarbons, Au-bearing fluids, and ground water, and the 10^1–10^2 m scale are important for understanding the growth of faults.

The purposes of this research were to (1) examine the fault structure of an inactive normal-fault zone with 50–100 m of throw that cuts a mixed carbonate and fine-grained clastic sequence, and (2) qualitatively evaluate the permeability structure of this fault zone. We use the setting of the fault in an ore deposit to provide geochemical markers that we use to show the relationship between faulting and fluid flow.

2. Geologic setting

Carlin gold deposits lie in northern Nevada and northwestern Utah, and Hofstra and Cline (2000) provide a thorough review of these deposits, from which most of the following overview is taken. Hofstra and Cline (2000) argue that Carlin deposits belong to their own unique class of ore deposits, owing to their paragenesis, age, structural setting, and likely mechanisms of formation. Carlin deposits are Paleozoic sedimentary rock hosted, with sub-micron gold disseminated in tabular or pod-like zones that are often spatially associated with faults. Depths of formation are greater than 2 km, at temperatures of 150–250 °C, in which hydrothermal fluids caused the dissolution of carbonate host rock, argillization of siliciclastics, sulfide deposition (and associated Au precipitation), and silicification of carbonates, creating jasperoids. Late-stage mineralization includes quartz, calcite, realgar, and barite (Arehart, 1996; Hofstra and Cline, 2000), and post ore mineralization consists of oxidation resulting in limonite and alunite formation.

The long and complex geologic history of the region includes Late Proterozoic rifting (Stewart, 1972), Paleozoic shallow marine sedimentation (Hose et al., 1976; Coats, 1987), foreland basin development of the Late Devonian–Early Mississippian Antler orogenic belt (Roberts et al., 1958; Gutschick and Rodriguez, 1979) and Jurassic and Cretaceous plutonism (Hudec, 1992; Hitchborn et al., 1996). Hinterland Cretaceous–early Tertiary Sevier contractional deformation (Armstrong, 1968), was followed by Eocene transpression and normal faulting (Nutt, 1996; Nutt and Good, 1998), which is likely the deformation event associated with the Casino deposit studied here (Nutt et al., 2000). The Alligator Ridge district is located at the southern end of the Ruby Mountain–East Humboldt Range metamorphic core complex and is located within the footwall of the Ruby listric fault (Snoke et al., 1997), the southern extension of the Ruby Mountains shear zone (Nutt et al., 2000). Younger (Middle Miocene to present), high-angle normal faults dissect the range (Mueller and Snoke, 1993; Nutt et al., 2000).

We examine the Keno fault, which is exposed by the abandoned Casino open-pit gold mine. The Casino pit lies at the northern end of the Alligator Ridge mining district

Fig. 1. Study area location and geologic maps. (A) North central Nevada is characterized by complexly faulted and folded Paleozoic shallow-marine rocks cut by normal faults throughout the region. (B) Large-scale geologic map of the study area. The Casino pit is located in the Bald Mountain–Alligator Ridge district, ~115 km south of Elko, Nevada. Tabular japeroid bodies lie within the Devonian sedimentary sequence of the Devil's Gate and Pilot Shales, which are cut by northeast- and northwest-trending faults. Ore deposits on the western side of the range are associated with the Jurassic pluton, and thought to have a different genesis than those in the Casino pit (Hammond, 2001; J. Brady, pers. commun., 2001). (C) Location of the study area in Nevada, relative to the Carlin gold trend. (D) Location of active or abandoned gold mines of the Alligator Ridge and Bald Mountain Districts. The open pit, disseminated gold deposits are scattered throughout the Bald Mountain–Alligator Ridge districts. Many of the deposits, including the Casino deposit, are spatially associated with faults. The region outlined by the dark box in (B) is based on unpublished mapping provided by Placer Dome, Inc.

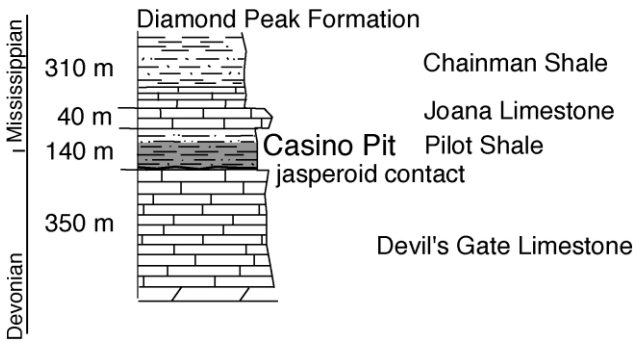

Fig. 2. Stratigraphy of Paleozoic rocks found within the study area (summarized from Hose et al. (1976), Ilchik et al. (1986), and Hitchborn et al. (1996)). Shading within the stratigraphic column represents the stratigraphic locations of the deposits in this study.

(Ilchik et al., 1986). Mining operations by Amax Mining, Inc. in the Casino pit provide a 350-m along-strike, 200-m across-strike, and 65-m down-dip exposure of a single, moderate-slip normal fault available for structural observations and geochemical sampling (Fig. 1). In this study, we present data on the architecture and permeability of this fault zone in siltstone and silty limestone collected from three transects within the pit.

The Casino deposit is a Carlin-type deposit in the Devonian–Mississippian lower Pilot Shale (Ilchik et al., 1986; Ilchik, 1990; Hitchborn et al., 1996; Stout, 1996; Nutt et al., 2000), which is a 140-m-thick, thin- to medium-bedded, siltstone and silty limestone (Nolan et al., 1956; Hose et al., 1976; Gutschick and Rodriguez, 1979; Fig. 2). Intense hydrothermal alteration throughout the deposit has destroyed much of the original, gently dipping bedding and protolith. Throughout the district, the contact between the Devil's Gate Limestone and Pilot Shale is brecciated and silicified (Klessig, 1984; Pancoast, 1986; Ilchik, 1990; Nutt et al., 2000). The Pilot Shale here consists of 80–90-m-thick lower sequence of thin-bedded illite–quartz siltstones and shales that are typically dolomitic where unaltered; the upper 50 m consist of medium bedded calcareous quartz–illite ± pyrite ± organic matter siltstone.

No mine records were available for the pit. The pit exposes the moderately east-dipping Keno normal fault, and there is abundant evidence for multiple periods of brecciation including fault and dissolution brecciation events. High-angle faults within the Bald Mountain–Alligator Ridge district have a complex history with many displaying both strike-slip and dip-slip sense-of-motion indicators and were probably reactivated multiple times from the Mesozoic to the Tertiary (Nutt, 1997; Nutt et al., 2000). Most faults strike either northwest or north-northeast, and north-northeast-striking faults usually cut northwest-striking faults (Nutt et al., 2000).

Gold deposits within the district are associated with high-angle faults, which are interpreted to have been pathways for Au-rich fluid migration (Ilchik, 1990; Hitchborn et al., 1996; Nutt et al., 2000). Similar fault-related deposits are found in Au deposits of northern Nevada (e.g. Rota, 1993; Volk et al., 1996; Hofstra and Cline, 2000). The detailed relationship between faults and Carlin-type deposits of the region is often unclear (Christensen, 1995). Some workers (e.g. Kuehn and Rose, 1992, their fig. 12; Arehart, 1996; Hofstra and Cline, 2000; Madrid and Roberts, 2001) indicate that faults are a conduit for fluid flow during mineralization, and several studies correlate Au with north- to northwest- and northeast-striking high-angle faults (Bagby and Berger, 1985; Jones and Huspeni, 1991; Teal and Jackson, 1997; Hofstra and Cline, 2000; Madrid and Roberts, 1991). Williams et al. (2000) documents the impact of faults in preparing the rocks for flow of mineralizing fluids. Some faults of the Carlin trend may postdate ore deposition and thus form a spatial, but not causal, relationship. Published literature (e.g. Volk et al., 1996; Williams et al., 2000) that present details on how faults influence the size, shape, and location of Au-deposits of the region, and their setting in the flow regime, are sparse.

Ilchik et al. (1986), Ilchik (1990), and Nutt et al. (2000) postulated that ore from the Alligator Ridge is stratabound within the deposits but northeast- and/or northwest-striking structures may have been utilized for ore-bearing fluid flow. The deposits are interpreted to have formed during the middle Eocene to early Oligocene (Ilchik, 1990; Hulen and Collister, 1999; Nutt et al., 2000), during the onset of extension in the study area (Nutt et al., 2000).

Numerous Au deposits within the Yankee basin at the southern end of the district host liquid hydrocarbons and pyrobitumen (Pinnell et al., 1991; Hulen et al., 1994; Hulen and Collister, 1999). Oil was first discovered within the Yankee open-pit mine (~30 km south of Casino) as coatings within fractures and hydrothermal veinlets (Pinnell et al., 1991) and has subsequently been identified within other deposits, mainly within fluid inclusions (Hulen et al., 1994; Hulen and Collister, 1999). Hulen et al. (1994) determined that the oil represents a relict petroleum reservoir, which has been destroyed by oxidation. The oil is thought to have migrated along high-angle faults (Pinnell et al., 1991) during the waning stages of Au mineralization (Hulen et al., 1994). It is commonly found within calcite veins and calcite-filled vugs, which are interpreted to have formed during late-stage, fluid-flow events associated with the Au deposition (Ilchik, 1990) and thus represent a second, late-stage phase of hydrocarbon generation and migration. Biomarkers and carbon isotope signatures suggest that the oils are self-sourced from the Pilot Shale (Hulen and Collister, 1999). Thus the Alligator Ridge deposits consist of a series of fluid-flow indicators that span the earliest stages of hydrothermal alteration to the cooler, post-ore mineralization phases of flow.

3. Methods

We performed a mesoscopic structural analysis and a whole-rock geochemical study to determine the geochemical and structural signature of the Keno fault zone. To

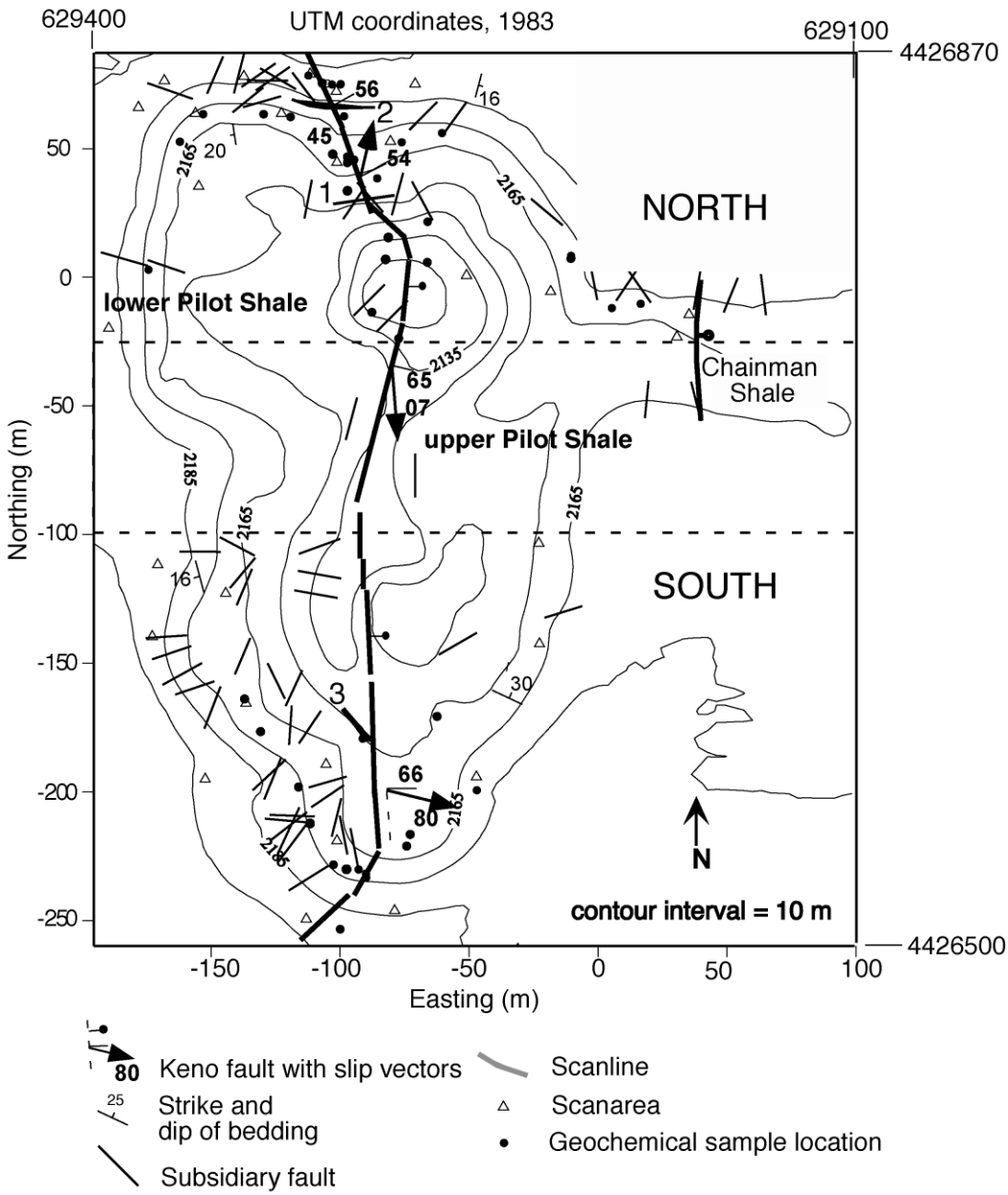

Fig. 3. Detailed geologic map of the Casino pit based on total station mapping. The Keno fault is exposed in the center of the pit and cuts the Mississippian–Devonian Pilot Shale. Subsidiary faults strike mainly northeast to north–south. Because the fault zone changes character along strike within the pit, the northern and southern exposures are described separately. All data collected north of the black dashed line are included in northern end investigations and data collected south of the southern black dashed line are included in the southern data set.

examine the spatial variability of fracture and fault density and orientations, we collected data on fractures and bedding planes ≥50 cm in trace length. These data included attitude, length, aperture, and coating by taking measurements along three linear transects that cross the fault zone. Linear and area fracture densities for fractures of all lengths were determined from twenty-six 1 m by 1 m scan areas and along the scanlines. We treat random errors due to measurement error, lighting, etc., by presenting the mean and standard deviations of densities assuming a normally distributed set of data. We do not account for orientation errors in linear sampling along scanlines that include higher rates of intersection for joints that are normal to the scanline than those that cross the line at lower angles, and fractures with longer trace lengths will intersect more scanlines (La Pointe and Hudson, 1985). The nearly vertical walls of the pit made it difficult to collect fracture data along vertical lines. Data on fault geometry, kinematics, relative timing, petrology, slip direction, and sense of motion were noted based on slickenline orientations or offsets of beds.

Forty-five samples were collected for geochemical analyses. Samples represent fault, breccia, vein, and altered

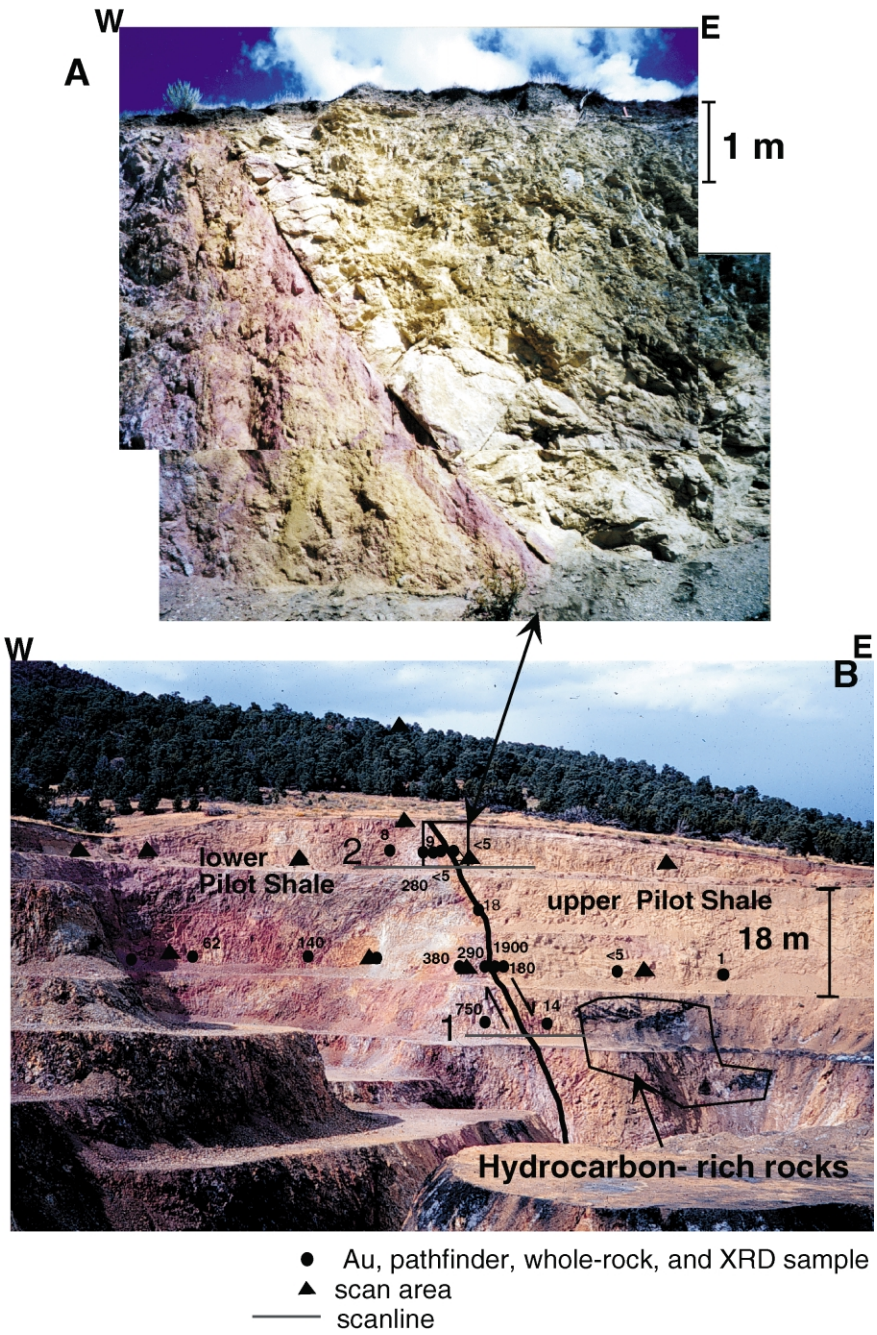

Fig. 4. Cross-sectional view northward of the northern end of the Casino deposit. The Keno fault is indicated by the line in (B), and consists of a single slip plane that is filled with 2 cm of gouge. Pods of pyrobitumen exist within the hanging wall of the fault and the footwall of the fault is marked by intense silicification. Note that in (A) rocks on either side of the fault are intensely fractured. The upper photo shows what appears to be a relatively unfractured block of Pilot Shale that is entrained within the fault zone. However, the only visible slip surface is the one that juxtaposes pink and tan rocks on the western side of the block. Whole-rock geochemical sample localities and Au content, in ppb, are shown.

but undeformed Pilot Shale. Plasma emission spectroscopy and X-ray fluorescence (XRF) analyses were completed by XRAL (Toronto, Canada) and Chemex (Elko, Nevada) to determine trace-element abundance and whole-rock concentrations. Gold in many Carlin deposits is accompanied by As, Sb, and Ag, and these elements are 'pathfinders' used for tracking the presence of Au and Au-bearing fluids. Fire assay and neutron activation analyses were completed by XRAL and Chemex to determine Au concentrations. We use the analyses of Ilchik (1990) for values of whole-rock compositions (and Au content) for unaltered Pilot shale. These data were collected for samples in the Vantage deposits, ~20 km south of the Casino pit. X-ray diffraction (XRD) analyses were completed to determine the mineralogy of the same samples analyzed for trace element and whole-rock compositions.

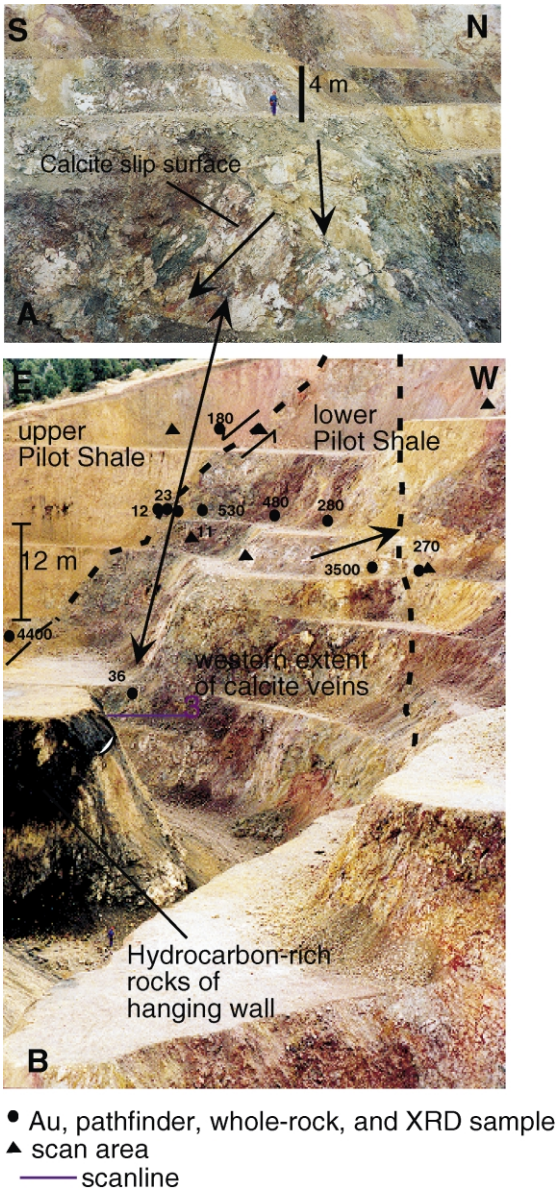

Fig. 5. (A) View to the west of a part of the footwall of the fault zone at the southern end of the pit. Slip indicators (arrows) show oblique slip and dip-slip along many calcite veins. (B) Cross-sectional view of the southern end of the Casino deposit. The fault is indicated by the solid line, and the fault zone consists of multiple large calcite veins that accommodated slip along the Keno fault, and a highly fractured zone in the footwall. Veins are up to 17 cm thick and contain liquid hydrocarbon. Whole-rock geochemical sample localities and Au content, in ppb, are shown.

Permeability analyses were conducted on Pilot Shale samples collected from within and near the Yankee deposits, ~30 km south of the Casino deposit, to determine the variance in permeabilities for altered and unaltered rocks. Axial permeabilities were measured on jacketed, cylindrical samples (3.7 cm diameter by 7.3 cm long) at Terra Tek, Inc., in Salt Lake City, Utah. Constant head tests for permeability to nitrogen gas were conducted at room temperature and pressure according to API standards.

4. Results

4.1. Deposit overview

We mapped the abandoned pit at a scale of 1:600 in order to determine the distribution and orientation of alteration assemblages, lithologies, and structures. Nearly all benches were accessible due to the lack of mining activity and few highwall failures. The pit extends 350 m north–south, 200 m east–west, and is 65 m deep (Fig. 3).

Siltstone and silty limestone of the Devonian–Mississippian Pilot Shale host the Casino deposit. Intense hydrothermal alteration throughout the deposit has destroyed much of the original, gently east-dipping bedding of the protolith. Hand-sample examination at the outcrop with hand lens and acid indicate that decalcification and silicification affected rocks throughout the deposit. The pit is bisected by a north–south-striking, moderately east-dipping normal fault, the Keno fault, and it contains at least 42 subsidiary high- and low-angle faults and numerous fractures. At least two periods of brecciation are found within the pit and include both fault and dissolution breccia. Pods of pyrobitumen are exposed in the hanging wall of the Keno fault and liquid hydrocarbons exist within calcite veins in the fault and its footwall. The Casino deposit is unusual for the district in that the Keno fault is well expressed in the pit, and there are few crosscutting structures of the deposit.

4.2. Mesoscopic fault-zone architecture

The best exposures of the fault are at the northern, 175-m-long (Fig. 4) and southern 110-m-long ends of the pit. The fault strikes north, dips range from 45 to 68° east, and juxtaposes the lower dolomitic, thin-bedded Pilot Shale in the footwall against upper calcitic, medium-bedding Pilot Shale in the hanging wall (Fig. 4). Footwall rocks are highly silicified and brecciated whereas hanging wall rocks are less silicified, fine-grained, thin- to medium-bedded siltstone and pods of pyrobitumen. Dip-slip displacement of the fault is constrained by the thicknesses of the units of the Pilot Shale and the vertical depth of the pit. Since only upper Pilot Shale is exposed in the hanging wall in the pit, and only lower Pilot Shale is in the footwall, the net dip-slip displacement is between 55 and 100 m. Slip vectors determined from slickenlines and grooved mineralized surfaces on the fault record three senses of motion: oblique normal slip at the northern end, strike-slip in the middle, and nearly pure dip-slip at the southern end (Fig. 3).

The Keno fault zone is a single slip surface at the northern end of the deposit (Fig. 4), and at the southern end of the fault the zone consists of numerous hydrocarbon-bearing calcite veins on which slip has occurred (Fig. 5). Because the fault is dramatically different at either end of the deposit, we discuss fault-zone architecture of the northern end of the fault zone separately from that of the southern end.

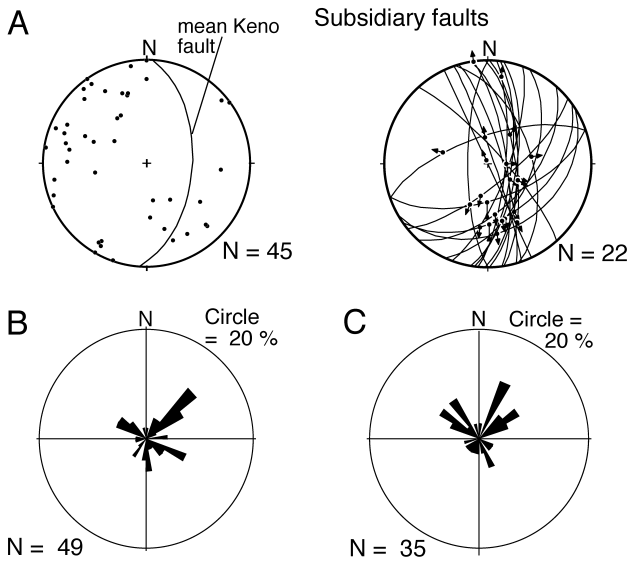

Fig. 6. Structural data from subsidiary faults and fractures within the Casino deposit plotted on lower hemisphere stereographic projections. (A) Fault orientation data. Poles to all faults are plotted on the left side, and faults on which slip sense was determined are plotted on the right side. Most faults within the deposit strike northeast to north–south and display oblique-slip indicators. (B) Rose diagrams of the strike of traces of fractures at the northern end of the pit, where most fractures strike northeast. (C) At the southern end of the deposit, fractures collected from scan areas generally strike northeast and northwest.

The hanging wall and footwall of the Keno fault contain subsidiary faults and innumerable fractures. The majority of the faults strike northeast to north–south but faults of other orientations also exist (Figs. 3 and 6). The presence of drag folds and offset markers suggests that faults are predominantly dip-slip. A north-striking fault at the entrance ramp on the eastern side of the pit juxtaposes Devonian–Mississippian upper Pilot Shale and Mississippian Chainman Shale (Fig. 3). Faults within the Casino pit, regardless of orientation, are often coated with a thin veneer of limonite or calcite. The limonite is likely a post-ore supergene alteration in the deposit.

4.2.1. Northern exposure

At its northern end, the Keno fault is a single, continuous, 10–20-mm-wide clay-rich gouge zone (Fig. 4), except on the highest bench (2183 m) within the pit. All slip appears to have been accommodated on this single gouge-filled plane. The rest of the 65 m of down-dip exposure of the fault is a single slip plane that juxtaposes lower and upper Pilot Shale and contains no entrained blocks. Outside of the narrow gouge zone, the rock is highly fractured but no apparent slip surfaces exist and no grain-size reduction of the Pilot Shale is visible in hand samples. We consider this thin gouge zone to be the structurally defined fault core.

Scanline data were collected across the fault core and into the adjacent rocks at two locations and scan area data from 16 locations at the northern end of the deposit (Fig. 3). Small faults strike northeast (Fig. 6a) whereas faults with discernible slickenlines strike north (Fig. 6b). Fractures strike northeast and northwest (Fig. 6c and d). Both sides of the fault are equally intensely fractured and there is no association between fracture density and distance from the fault core across the 235-m region examined perpendicular to the fault zone (Fig. 7).

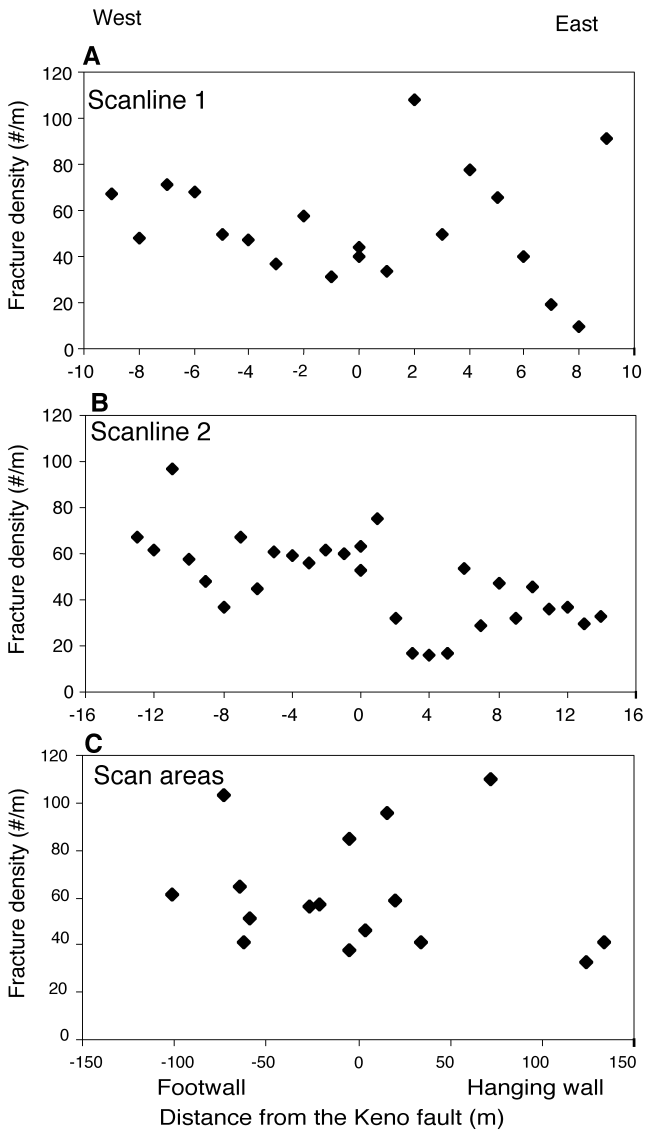

Fig. 7. Fracture densities from the northern end of Casino deposit. See Figs. 3 and 4 for locations of scan lines and scan areas. Within the footwall of each data set, there is a slight increase in fracture density away from the fault. Hanging wall densities from scanline 1 and the scan area data show no trend with increasing distance from the fault and exhibit more fracture density variability than the footwall. Scanline 2 densities decrease with increasing distance from the fault.

Most fracture trace lengths are $\leq$10 cm. The maximum density of fractures is 108 fractures/m, with the average being 49. Fractures $\geq$50 cm long tend to have a 1- to 3-mm aperture, terminate into other fractures (high connectivity), contain no coating, and exhibit no association between trace length and aperture. Neither aperture nor trace length increases near the fault (Fig. 8).

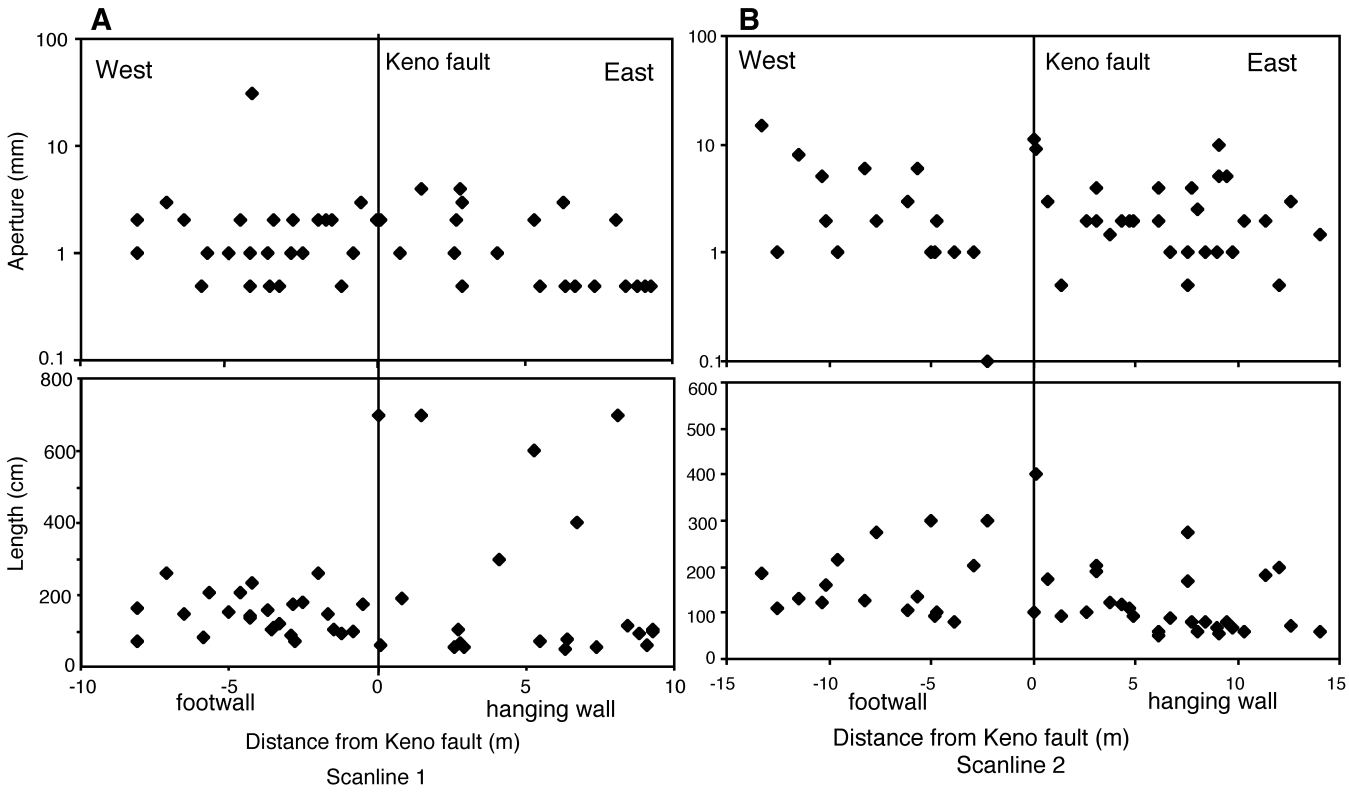

Fig. 8. Fracture aperture and trace length with respect to distance from the Keno fault. No association with distance to the fault zone exists within either data set.

4.2.2. Southern exposure

The southern exposure consists of tens of steeply dipping, 5- to 170-mm-wide calcite veins with slickensides on them (Fig. 5). Textures and slickensides within the calcite veins indicate that multiple slip events occurred along many of the veins, suggesting that they accommodated the slip that was accommodated by a single fault plane to the north. The presence of slip indicators on the calcite veins, which are interpreted to have formed during late-stage fluid-flow events (Ilchik, 1990; Hulen et al., 1994), shows that the fault slipped late within the history of the deposit. Between the calcite veins, the Pilot Shale is silicified, brecciated, and fractured. Multiple periods of brecciation are evident as some breccia clasts contain older breccia. We interpret the structurally defined fault core to be the area between the eastern and western extent of calcite veins, an ~20-m-wide zone (Fig. 5). Rocks in the hanging wall are tan and highly fractured, similar to rocks in the hanging wall at the northern end of the deposit. Rocks in the footwall are silicified similar to the footwall rocks at the northern end of the deposit.

Fracture data collected along a 15-m-long scanline within the fault zone at the southern end of the deposit show that fracture density increases slightly toward large limonite or calcite-filled fractures, followed by a sharp decrease (Fig. 9a). Fractures ≥50 cm in trace length tend to have ≤3-mm apertures, generally connect with other fractures where they terminate, and are coated or filled either with calcite or are uncoated. No relationship exists between aperture or trace length and distance from the eastern extent of the fault core (Fig. 9b and c).

Fracture data were also collected from 12 scan areas across a 140-m transect at a high angle to the Keno fault (Figs. 2 and 10). Fractures predominantly strike northwest and northeast (Fig. 6). Fracture density data show no discernible relations in either the footwall or the hanging wall (Fig. 10). No trend exists within the hanging wall (Fig. 10), although the data are limited. Data from the far end of the area may represent a background value of 30–40 fractures/m in the Pilot Shale (Fig. 10). Thus, either a fault-related damaged zone does not exist, or is masked by the dense fracturing of the entire deposit, or is up to 160 m wide.

4.3. Geochemically defined fault zone

Twenty-nine samples from the northern end and 16 samples from the southern end of the deposit (see Figs. 3–5 for sample locations) were analyzed for trace-element (Au and pathfinder), whole-rock, and mineral content in order to determine the fluid-flow indicators and fault-zone permeability. For these purposes, we first consider the fault simply as the plane that separates upper and lower Pilot Shale, and then examine how pathfinder and whole-rock analyses compare with the location of the fault zone.

Fresh, unaltered samples of lower Pilot Shale from the vicinity of the Vantage deposits have a normative mineralogy of 35–50% illite, 30–45% dolomite + calcite, 14%

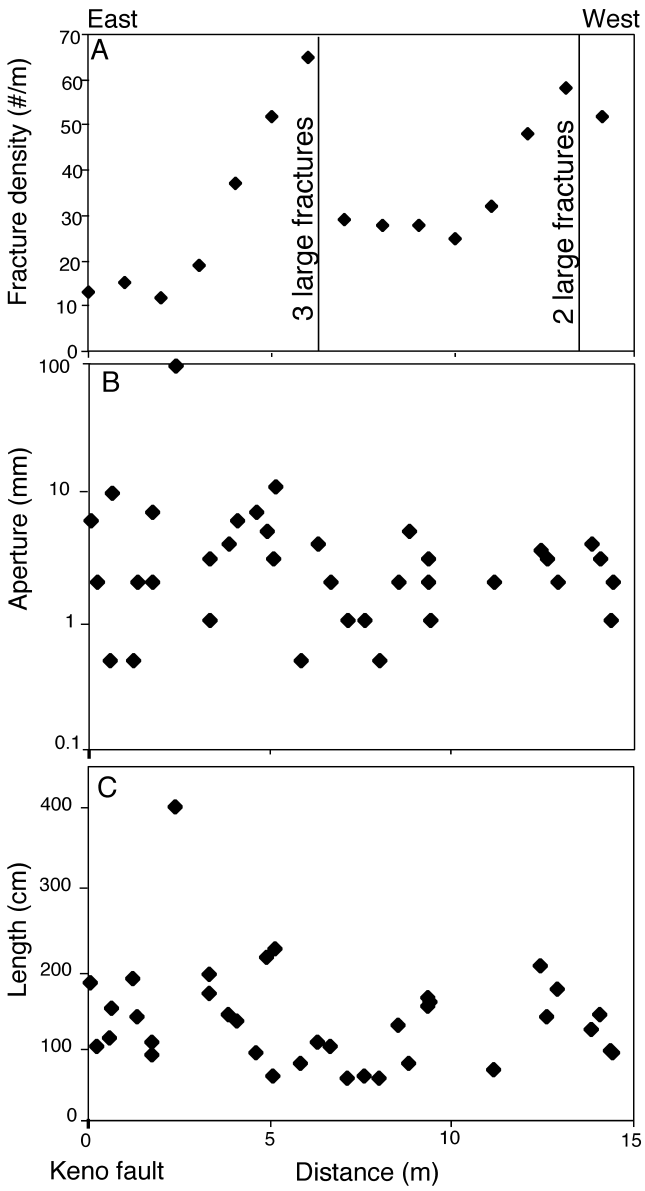

Fig. 9. Fracture data from scanline 3. Neither fracture density (A), aperture (B), nor length (C) is associated with distance from the eastern extent of the Keno fault core towards the footwall. Fracture density increases on either side of clusters of large fractures, perhaps reflecting a direct relationship between fracture density and faulting that has been described in other studies (e.g. Chester and Logan, 1986).

detrital quartz, 5% pyrite, 1.5% organic matter, and 0–3% kaolinite (all in weight percent) (Ilchik, 1990). Trace-element analyses reveal that unaltered Pilot Shale from the same area contains <0.005 ppm Au, 40 ppm As, and 10 ppm Sb (Ilchik, 1990). We assume that unaltered Pilot Shale from the Casino region had similar mineral and elemental assemblages as that from the Vantage area, which is ~20 km south of Casino.

Trace-element analyses show that overall the Casino deposit is a low-grade Au deposit (<5–15,000 ppb) that contains elevated concentrations of As and Sb (Table 1). We use these elements as fluid-flow indicators during main-stage mineralization. Interpretation of the whole-rock geochemiical analyses (Table 2) and XRD analyses show that this deposit has been enriched in quartz and depleted in calcite and dolomite.

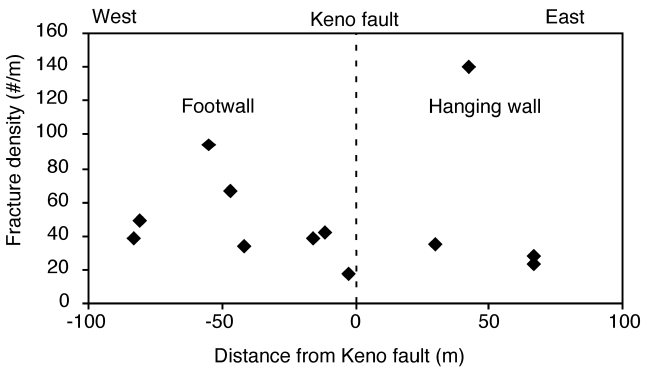

Fig. 10. Fracture densities from scan area data collected from the southern end of Casino deposit. Within the footwall, fracture densities increase with increasing distance from the Keno fault. The limited hanging wall data reveal no trend between density and increasing distance from the fault.

The northern end of the fault has a distinct geochemical signature where SiO_2 changes dramatically across the fault with 70–80% values in the footwall, and 30–40% in the hanging wall (Fig. 11). Conversely, (CaO + MgO) are nearly zero in the footwall, and lie in the 20% range in the hanging wall. Values of Al_2O_3 appear to increase towards the fault, but no other major element analyses exhibits a discernible trend. The pathfinder analyses also show an abrupt transition that lies in the hanging wall of the fault (Fig. 11). Gold contents drop from 1900 ppb in the footwall (baseline is 40 ppb) to 52 ppb in the hanging wall; As and Sb decrease by factors of 3 and 8, respectively, across the fault. The highest value of gold in the pit (15,000 ppb) is found in a fault gouge sample.

We use these data to test the hypothesis that the Keno fault simply cuts a pre-existing Au-bearing silicified deposit. A detailed examination of the data shows that the elevated pathfinder content extends at least 7.9 m into the hanging wall, and high SiO_2 values exist at 3.8 m into the hanging wall. These data suggest that Au mineralization was related to the fault, and that the fault does not simply cut a pre-existing Au deposit.

The gold, SiO_2, and pathfinder element signature at the southern end of the pit is more complex. Average gold values are higher in the hanging wall than in the footwall of the fault (Fig. 12a), and gold is lower within the fault samples than either footwall or hanging wall samples. Pathfinder elements are slightly different across the fault zone, but are all well above background levels. The silicification of the hanging wall develops about 10 m from the fault zone in the hanging wall and continues across the fault zone.

Thus, as in the case at the northern exposure, we interpret these results to show that the fault does not cut an older deposit, but was related to the flow of the SiO_2 and Au-bearing fluids that formed the deposit. The southern end of

Table 1
Au and pathfinder composition of the Casino deposit

Sample type	Sample no.	Distance from Keno fault (m)	Au (ppb)	As (ppm)	Sb (ppm)
Northern end of the deposit					
Footwall of Keno fault (Pilot Shale)	ZS40	78.1	<5	100	180
	ZS41	66.2	44	67	96
	ZS42	57.1	62	470	350
	ZS43b	34.5	140	720	1600
	ZS44	23.0	120	510	110
	ZS86	12.4	460	290	220
	ZS69	11.8	750	170	240
	ZS90	7.9	710	140	150
	ZS46	7.7	380	800	420
	ZS20	7.2	8	430	270
	ZS47	4.1	2900	230	44
	ZS21	1.8	280	590	85
	ZS85b	1.1	15,000	1700	1100
	ZS21b	0.7	9	510	24
Keno fault	KFS4	0	18	29	8.8
	ZFS21-22	0	<5	350	89
	ZFS47-48	0	1900	640	230
	ZFS84	0	780	680	200
Hanging wall of Keno fault (Pilot Shale)	ZS48	0.6	180	410	26
	ZFS71-72	3.3	14	340	25
	ZS87	3.8	230	95	260
	ZS22	5.4	<5	27	3.9
	ZS91a	7.9	110	720	110
	ZFS49a	19.3	5	60	5.7
	ZFS49b	35.0	16	36	4.5
	ZS50c	86.6	<5	120	4.5
	ZS50a	86.7	5	41	4
	ZS51	102.5	<5	10	2.1
	ZS52a	113.8	16	170	15
Southern end of the deposit					
Footwall of Keno fault (Pilot Shale)	ZS36	47.6	270	170	110
	ZS35	42.9	3500	2200	570
	ZS34	25.9	280	170	240
	ZFS32e	21.4	480	810	940
	32E	21.4	197	386	386
	ZS32b	12.2	140	270	720
	ZS32a	7.1	530	260	54
	ZFS79e	6.1	36	720	330
	79E	6.1	11	241	112
Keno fault	KFS6	0	11	880	94
	ZFS31-32	0	23	840	60
Hanging wall of Keno fault (Pilot Shale)	ZS62b	9.7	4400	670	360
	ZS2a	10.6	180	490	66
	ZFS79a	10.7	690	540	360
	ZF76-77	21.5	1800	230	22
	ZS30a	43.2	12	220	5.9

the fault appears to have formed a broader zone of mineralization.

We test the hypothesis that the SiO_2 and Au-bearing fluid were related to fracture densities in the hanging wall and footwall across the northern and southern sites (Fig. 13). The data show that there is no correlation whatsoever between the Au content and fracture density that we can measure today. Thus, the fluids were introduced along fractures and in the rock matrix, and fractures that developed during or after mineralization have masked the effect, or the ore-bearing fluids had a high degree of matrix-dominated flow. Hammond (2001) performed a variety of multivariable statistical tests to determine if any correlation may exist between the signatures of fluid flow and fracture densities, and none were found.

4.4. Microstructures

The microstructures of the fault zone from the northern end of the fault (Fig. 14) show the wide range of textures that developed during faulting. The northern end of the fault zone is expressed by narrow, well-developed clay-rich fault

Table 2
Whole-rock composition of the Casino deposit

Sample type	Sample no.	Distance from Keno fault (m)	Weight percent											
			SiO_2	Al_2O_3	CaO	MgO	Na_2O	K_2O	Fe_2O_3	MnO	TiO_2	P_2O_5	Cr_2O_3	LOI
Northern end of the deposit														
Footwall of Keno fault (Pilot Shale)	ZS40	78.1	82.3	8.48	0.35	0.61	0.03	1.61	2.94	<0.01	0.56	0.2	<0.01	2.95
	ZS41	66.2	88	5.69	0.26	0.52	<0.01	1.08	2.53	<0.01	0.28	0.1	0.02	1.90
	ZS42	57.1	72.4	8.54	3.39	2.86	<0.01	1.8	3.61	<0.01	0.44	0.16	<0.01	7.15
	ZS43b	34.5	77.8	10	0.32	0.84	0.01	2	4.78	<0.01	0.53	0.12	0.01	3.75
	ZS44	23.0	75.8	7.1	4.14	1.53	<0.01	1.21	3.27	<0.01	0.33	0.18	<0.01	6.50
	ZS86	12.4	85.7	5.43	0.16	0.36	0.02	1.18	2.78	<0.01	0.16	0.09	0.01	3.70
	ZS69	11.8	83.6	7.7	0.11	0.25	<0.01	1.26	2.16	<0.01	0.44	0.13	0.02	4.45
	ZS90	7.9	87.5	4.15	0.2	0.16	<0.01	0.6	2.61	<0.01	0.07	0.1	0.05	1.80
	ZS46	7.7	70.4	13.1	0.24	1.08	0.02	2.27	5.62	0.03	0.51	0.23	0.02	5.35
	ZS20	7.2	81.2	6.92	0.61	0.2	0.05	1.24	4.23	<0.01	0.41	0.17	0.02	5.05
	ZS47	4.1	78.3	9.59	0.35	0.51	0.02	1.73	3.86	<0.01	0.44	0.18	0.02	4.85
	ZS21	1.8	67.7	10.5	5.9	0.91	0.05	1.71	4.45	<0.01	0.52	0.13	0.01	8.45
	ZS85b	1.1	26.8	29.3	0.28	0.18	0.57	7.3	4.28	<0.01	0.07	0.34	0.02	30.40
	ZS21b	0.7	65.3	12.1	3.07	2.58	0.02	1.96	4.65	0.02	0.46	0.19	0.01	8.35
Keno fault	KFS4	0	11.7	2.47	42.9	3.31	<0.01	0.5	1.23	<0.01	0.14	0.03	<0.01	38.30
	ZFS21-22	0	59.5	11.3	2.66	1.38	0.19	1.87	5.92	<0.01	0.54	0.14	<0.01	6.80
	ZFS47-48	0	70.5	14.2	0.65	0.64	<0.01	0.82	5.82	<0.01	0.76	0.18	0.02	6.55
	ZFS84	0	75.7	9.63	0.39	0.22	0.01	1.52	6	<0.01	0.54	0.12	0.02	6.00
Hanging wall of Keno fault (Pilot Shale)	ZS48	0.6	69.3	14.4	0.62	1.06	0.06	1.85	5.58	<0.01	0.67	0.22	0.01	6.30
	ZFS71-72	3.3	45.6	8.91	16.6	3.66	<0.01	1.6	4.16	0.03	0.46	0.1	<0.01	19.10
	ZS87	3.8	85.4	7.07	0.44	0.29	<0.01	1.14	2.66	<0.01	0.46	0.17	0.02	2.55
	ZS22	5.4	35.2	8.02	16.6	9.3	0.05	2.15	3.43	0.06	0.48	0.09	<0.01	25.30
	ZS91a	7.9	34.2	6.86	26.9	1.01	0.01	1.34	5.05	<0.01	0.21	0.07	0.01	24.50
	ZFS49a	19.3	42.8	9.61	12.2	7.7	0.03	1.94	4.71	0.06	0.57	0.11	0.01	20.70
	ZFS49b	35.0	49.9	13.1	10.2	3.89	0.05	2.38	4.3	0.01	0.77	0.14	0.02	15.90
	ZS50c	86.6	39.5	8.96	14.2	8.49	0.08	1.94	3.46	0.05	0.52	0.1	0.01	22.80
	ZS50a	86.7	49.6	10.2	9.35	6.54	0.06	2.4	4.38	0.03	0.56	0.15	0.01	17.10
	ZS51	102.5	33.7	6.05	16.9	11.2	0.06	1.75	2.68	0.07	0.34	0.1	<0.01	27.40
	ZS52a	113.8	89.2	3.07	0.29	0.34	<0.01	0.71	3.9	<0.01	0.17	0.07	0.04	2.30
Southern end of the deposit														
Footwall of Keno fault (Pilot Shale)	ZS36	47.6	80.2	5.53	0.03	0.25	0.12	0.67	2.8	<0.01	0.21	0.14	<0.01	1.90
	ZS35	42.9	63.4	12.9	0.8	0.1	<0.01	0.16	12.6	<0.01	1.53	0.65	0.1	7.80
	ZS34	25.9	87.7	5.72	0.2	0.2	<0.01	0.6	3.6	<0.01	0.25	0.19	0.03	1.85
	ZFS32e	21.4	80.9	3.17	0.38	0.28	<0.01	0.47	12.1	0.02	0.19	0.11	0.04	1.70
	32E	21.4	81.35	3.83	0.31	0.11	0.07	0.67	9.44	0.01	0.15	0.15	0.03	2.80
	ZS32b	12.2	83.8	4.18	2.74	0.21	<0.01	0.49	4.95	0.01	0.03	0.12	0.05	2.65
	ZS32a	7.1	88.2	5.16	0.64	0.26	<0.01	0.85	2.38	<0.01	0.32	0.1	0.02	2.25
	79E	6.1	86.85	1.53	1.05	0.02	0.09	0.13	4.87	0.01	0.05	0.07	0.03	1.22
	ZFS79e	6.1	79.5	1.56	4.89	0.07	0.01	0.16	7.06	0.02	<0.01	0.11	0.05	3.15
Keno fault	KFS6	0	64	11	5.44	2.75	0.03	1.88	4.64	0.03	0.54	0.17	0.01	9.70
	ZFS31-32	0	62.9	9.56	8.09	2.61	0.02	1.52	3.69	0.01	0.49	0.14	0.02	11.30

(*continued on next page*)

Table 2 (*continued*)

Sample type	Sample no.	Distance from Keno fault (m)	Weight percent										
			SiO_2	Al_2O_3	CaO	MgO	Na_2O	K_2O	Fe_2O_3	MnO	TiO_2	P_2O_5	Cr_2O_3	LOI
Hanging wall of Keno fault (Pilot Shale)	ZS62b	9.7	82.4	8.49	0.41	0.57	<0.01	1.15	3.08	<0.01	0.45	0.11	0.01	3.60
	ZS2a	10.6	75.2	11.3	0.31	1.12	0.05	2.29	4.17	<0.01	0.58	0.16	0.01	4.85
	ZFS79a	10.7	39	4.83	26.4	0.61	<0.01	0.71	4.9	<0.01	0.27	0.15	0.01	22.60
	ZF76-77	21.5	29.2	5.06	33.3	0.77	<0.01	0.92	2.11	<0.01	0.29	0.1	<0.01	28.40
	ZS30a	43.2	65.6	8.61	5.05	3.55	0.03	2.38	4.62	0.02	0.40	0.27	<0.01	9.70

gouge in the siltstone (Fig. 14a). Here comminuted quartz grains lie in a fine-grained matrix of clay, and a foliation is defined by anastomosing dark slip surfaces. Calcite veins are thin and tend to parallel the foliation of the fault zone (Fig. 14b and c). At the southern end of the fault, the relationship between fault gouge and late-stage flow supports an interpretation of high fluid pressures, which caused calcite-rich fluids to be injected into the gouge (Fig. 14d and e). Veins form random fabric breccias with the clasts composed of angular fragments of fine-grained gouge (Fig. 14e), which in some cases appear to form in several stages (Fig. 14d). SEM images of the vein and gouge textures (Fig. 14f) show grains of stibnite and barite (thought to be late ore stage; Hofstra and Cline, 2000) cut by fine-grained gouge, and calcite veins cut both the gouge and the late-stage ore minerals.

4.5. Permeability analyses

Permeability analyses were conducted on both unaltered and altered Pilot Shale from the West Crusher pit, ~30 km south of the Casino deposit. The bulk rock permeability of unaltered Pilot Shale is 6.2×10^{-17} m^2, whereas silicified Pilot Shale is 6.4×10^{-18} m^2. Jasperoid from the Devil's Gate Limestone–Pilot Shale contact has a permeability of 1.4×10^{-18} m^2. Each of these values is similar to that of clay gouge ($\leq 10^{-18}$ m^2; Morrow et al., 1984). Forster et al. (1999) computed a modeled macroscopic permeability for fractured Pilot Shale. They assumed fractures of 1-mm aperture, linear fracture densities of 75–100/m, no matrix permeability and used a discrete fracture flow model to determine that intensely fractured Pilot Shale has a permeability of 4.9×10^{-13} m^2 for blocks 10 m on a side. The results of these analyses suggest that Au-bearing fluid flow would have been concentrated in intensely fractured areas within the Casino deposit.

5. Interpretation

The data provided here document the geochemical and structural nature of the Keno fault zone. The signature of the fault zone varies depending on the type of analysis used and on the location along the fault (Fig. 15). At the northern end of the deposit, structural analyses show that the fault core is ≤ 20 mm thick. Whole-rock geochemical indicators define a narrow fault zone in which gold values are highest near the fault core and decrease away from the fault, and SiO_2 values change dramatically from one side of the fault core to the next but are not offset by the fault itself.

The physically based fault zone at the southern end of the deposit is the same width as the geochemically defined fault zone at the northern end. The fault core is composed of a 15-m-wide zone of calcite-filled veins. Rocks in the hanging wall and footwall are intensely fractured and again, we could not determine the full extent of deformation

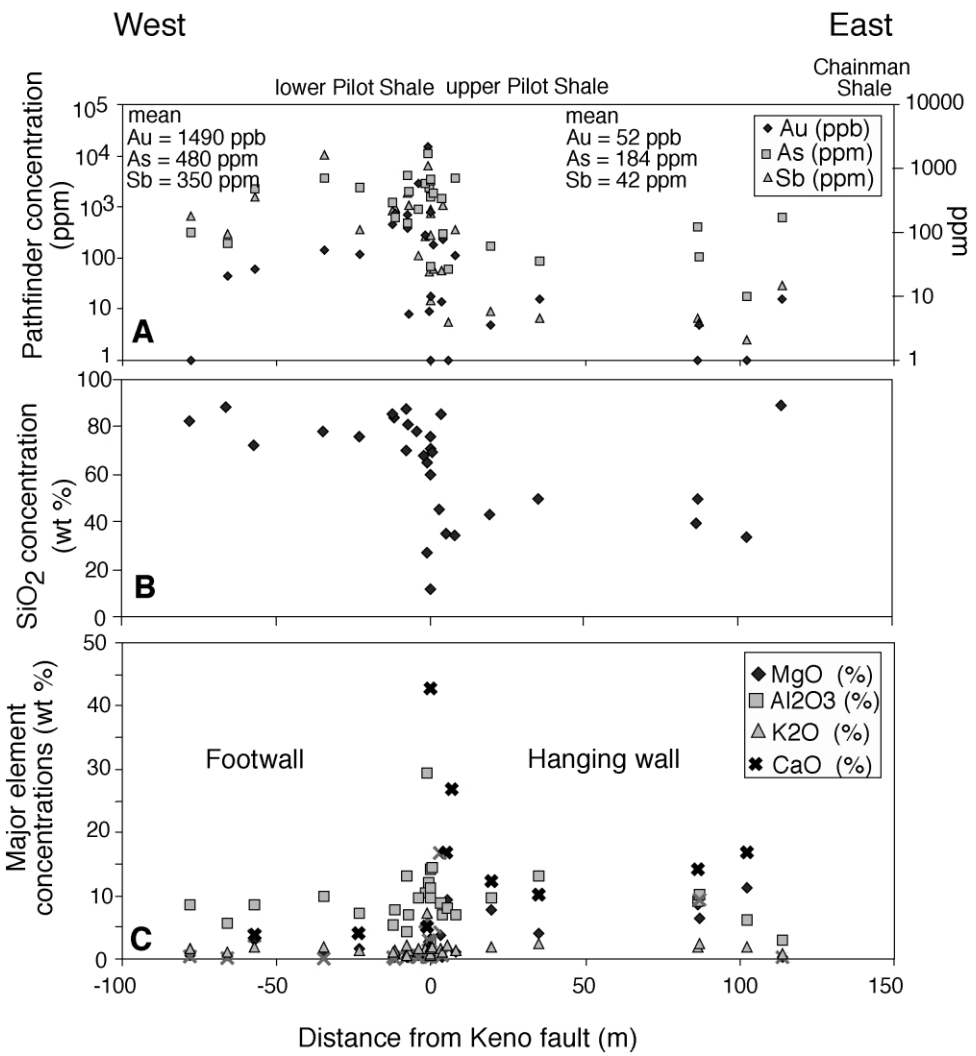

Fig. 11. Geochemical data from the northern end of the Casino deposit. Concentrations of Au, As, and Sb are higher in the footwall than in the hanging wall and decrease with increasing distance from the slip surface (A). There is also more SiO_2 within the footwall than the hanging wall but values do not vary with increasing distance from the fault (B). MgO and CaO concentrations are higher within the hanging wall than the footwall (C).

associated with slip along the Keno fault. Gold, pathfinder elements, and SiO_2 do not vary significantly across the fault. The fault is associated with changes in Al_2O_3 and CaO abundance, which decreases from the fault to 20 m into the footwall. Based on all indicators, the Keno fault is $\leq$20 m wide at the southern end of the deposit.

While there is a geochemical signature to the fault zone that appears consistent with the fault acting as a conduit for hydrothermal fluids, there is little structural signature of the fault zone. Fracture densities across the fault zone are indistiguishable, and likely reflect the long, complex structural history of the area as well as fractures that are related to volume reductions associated with silicification. The lack of a structurally defined damaged zone may be due to undersampling of fracture densities away from the fault zone—that is, perhaps the width of the fault damaged zone $>$160 m. Comparison of background fracture values in the same rocks from the Alligator Ridge district (Schulz et al., 1998) argue against that. The numerous deformation events, alteration, and the nature of the protolith lithologies have combined to create a planar fault that developed in a relatively weak, pre-fractured rock mass before the Keno fault formed. Thus, strain could be accumulated along the fault without significant damage being accumulated in a zone around the fault.

Our work also shows that the fault zone is structurally and compositionally heterogeneous along strike and the fault thickness and mineral fillings may vary over short distances. It is not clear why these variations exist along the Keno fault. It is possible that we are observing the results of fault growth from small to moderate slip, and thus see the superposition of fault tip structures with fault structures near the center of a fault (Morewood and Roberts, 2000).

We suggest that the fault was a distributed conduit to fluid flow at both ends of the pit early in its history, having provided a vertical connection through a complexly deformed rock mass (Forster et al., 1999). The intense fracturing that existed before faulting may have combined

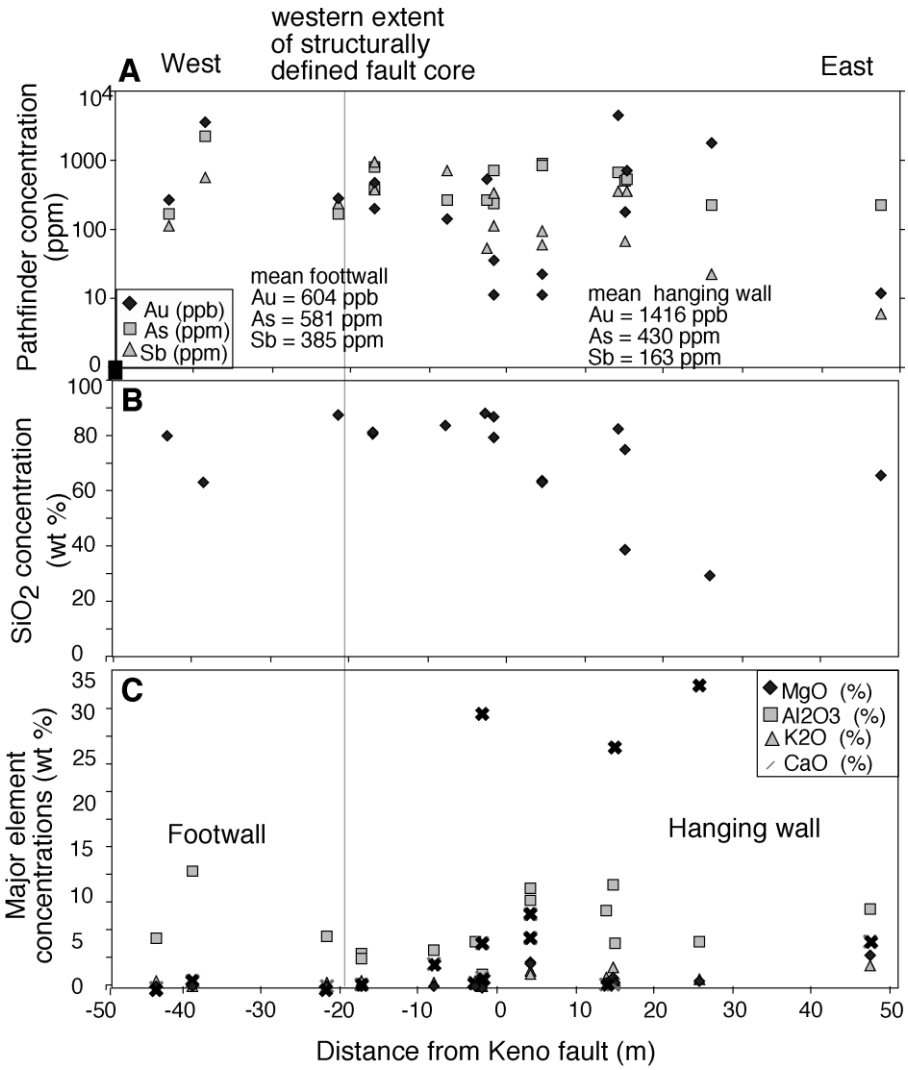

Fig. 12. Geochemical data from the southern end of the Casino deposit. Concentrations of Au and As are higher within the hanging wall than the footwall (A). Au increases with increasing distance from the fault in the footwall but decreases, along with As and Sb, within the hanging wall (A). SiO_2 concentrations are similar within the footwall and hanging wall and decrease with increasing distance from the fault (B). MgO and CaO concentrations are higher within the hanging wall than the footwall (C).

with fractures that were created during faulting to provide permeable pathways for fluid flow. However, the permeability changed from that of a distributed conduit to a combined conduit-barrier with increased slip at the northern end of the deposit, where concentrations of Au, pathfinder elements, and SiO_2 are considerably higher than within the hanging wall.

Based on the distribution of Au and pathfinder elements, Au-bearing fluids likely flowed from depth along the Keno fault at the northern end of the deposit and into intensely fractured hanging wall and footwall rocks of the Pilot Shale during its earliest stages of development when little or no clay gouge was present. Fluid flow across the fault was prevented as the clay fault gouge, which may have had permeabilities from 10^{-22} to 10^{-18} m^2 (Morrow et al., 1984), developed. The fault gouge was created as the fault slipped by comminution of wall rocks and diagenesis caused by fluid flow. Although the gouge was relatively thin ($\leq$20 mm), its continuity made it an effective barrier (e.g. Yielding et al., 1997). Subsequent mineralization was largely confined to the footwall where fluids traveled updip along bedding and fractures of higher permeability to regions of lower pressure. Changes in permeability structure such as this would be indeterminable without fluid-flow indicators such as trace elements. Late-stage barite–calcite veins formed in the footwall of the fault at the southern end, and these deposits were superimposed on flow of liquid hydrocarbon (J.G. Solum, pers. commun., 2002).

Our objectives of this research were to test the hypotheses that there would be a distinct correlation at the deposit-scale, and the meter-scale, between fracture density and the presence of the fault, and between fracture density and the presence of gold or its related trace elements. Within the Alligator Ridge district, south of the Casino deposit,

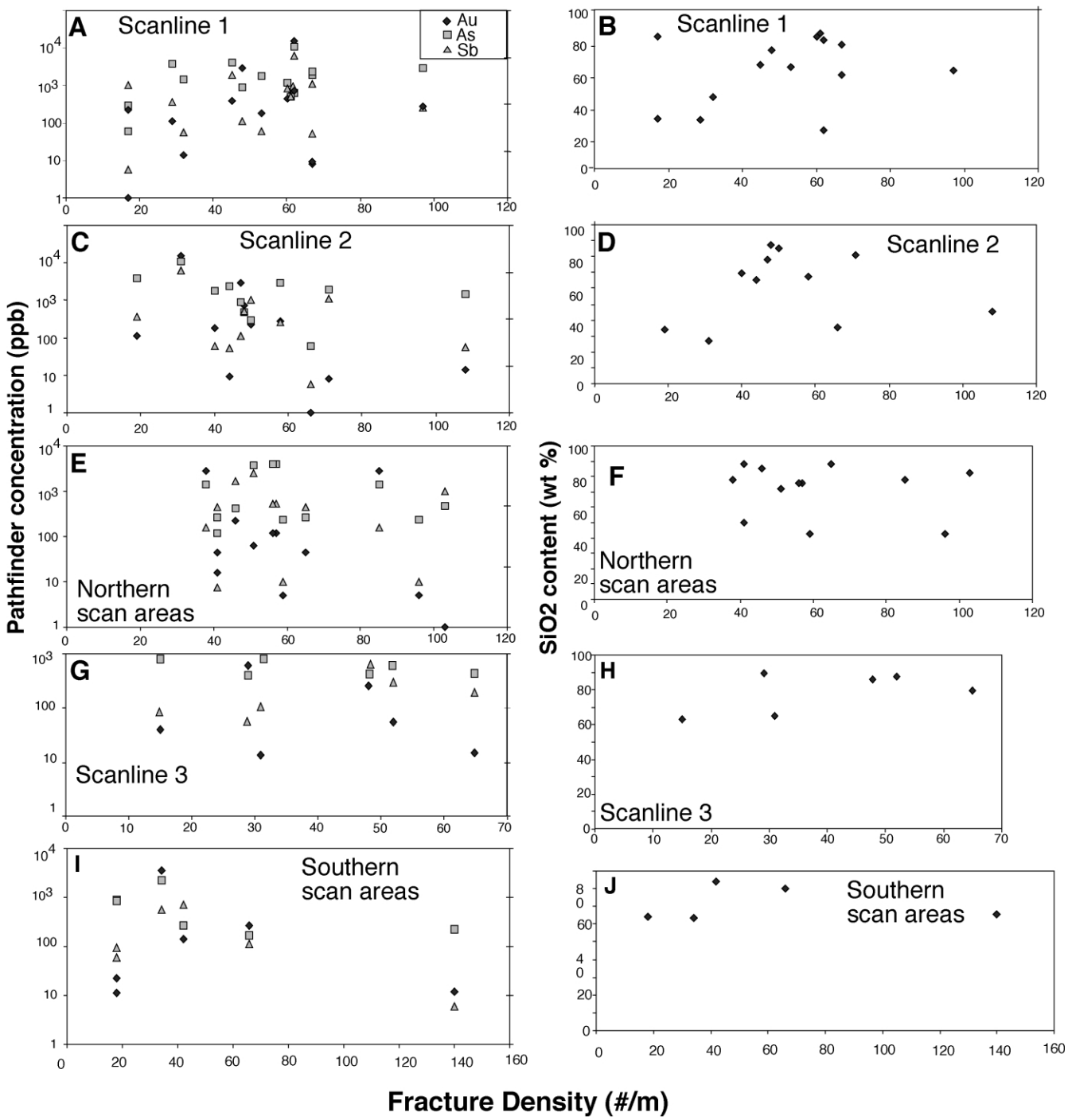

Fig. 13. Geochemical concentrations with respect to fracture densities from the study area. Pathfinder and SiO_2 concentrations as function of fracture densities for scanline 1 (A, B); scanline 2 (C, D); northern scan areas (E, F); scanline 3 (G, H); southern scan areas (I, J).

Schulz et al. (1998) found an association between fracture densities and trace-element concentrations, as have others for intrusion-related deposits (Titley et al., 1986; Hammond, 2001). We found little evidence for a damaged zone that scales with the fault length or total slip; rather the entire deposit is characterized by a densely fractured and altered sequence of rock. Gold and pathfinder concentrations are grossly correlated with the fault zone at the pit scale, but do not correlate well at the fine scale. This has been documented in other Carlin deposits as well, where 'structural control' on a deposit is true at the pit scale, but deviates at the meter or tens of meter scales (see, for example, Stenger et al., 1998; Figs. 1–5). It may that the nature and rates of the reactions that occur in these Carlin deposits, coupled with the very fine-grained nature of the mineralization that must be responsible for the dissemination

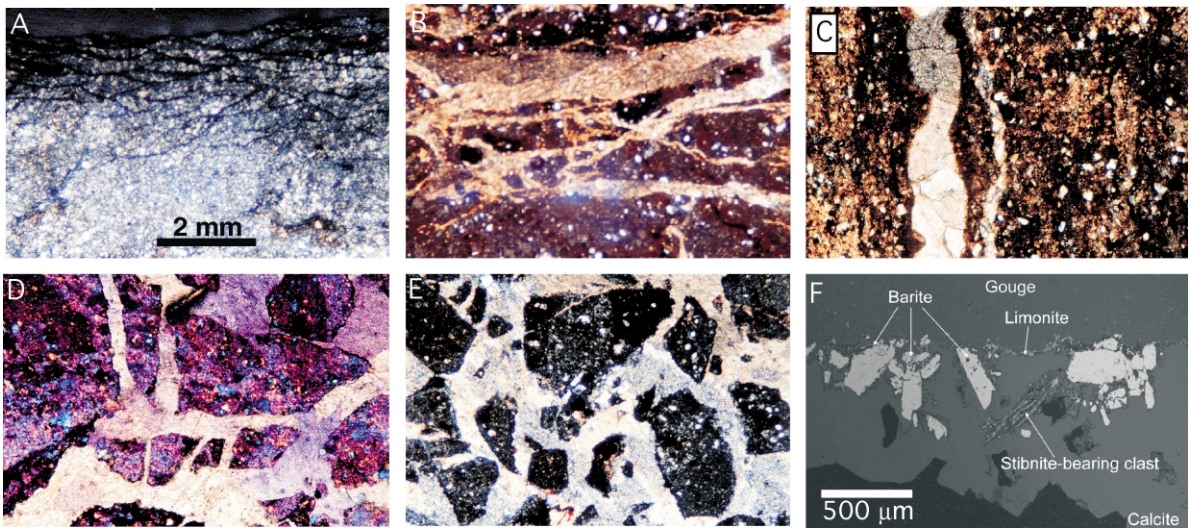

Fig. 14. Representative microstructures of fault-related rocks from the Keno fault. For figures A–E, scale bar shown in (A). (A) Cross-polarized photomicrograph of clay-rich fault zone at northern end of the pit. Thin clay-gouge marked by interleaving zones of gouge in a siltstone matrix. (B) Cross-polarized photomicrograph of subplanar calcite veins cut clay gouge. (C) Cross-polarized photomicrograph of veins that in some cases follow the foliation defined in the gouge. (D) Cross-polarized photomicrograph with 1/4 wave plate from fault zone sample at the southern end of the pit, where networks of calcite veins (lightest color) cut calcite–barite veins (light pink) that cut brown gouge. (E) Cross-polarized photomicrographs showing that relatively high pore-fluid pressure existed during calcite vein formation are suggested by clasts of gouge supported by calcite. (F) Back-scattered SEM image of vein showing clay gouge (top) cut by a calcite vein that contains barite and a stibnite clast. The stibnite clast was deposited at higher temperature and was incorporated into the vein by later calcite-rich fluid. BSEM image provide by J.G. Solum.

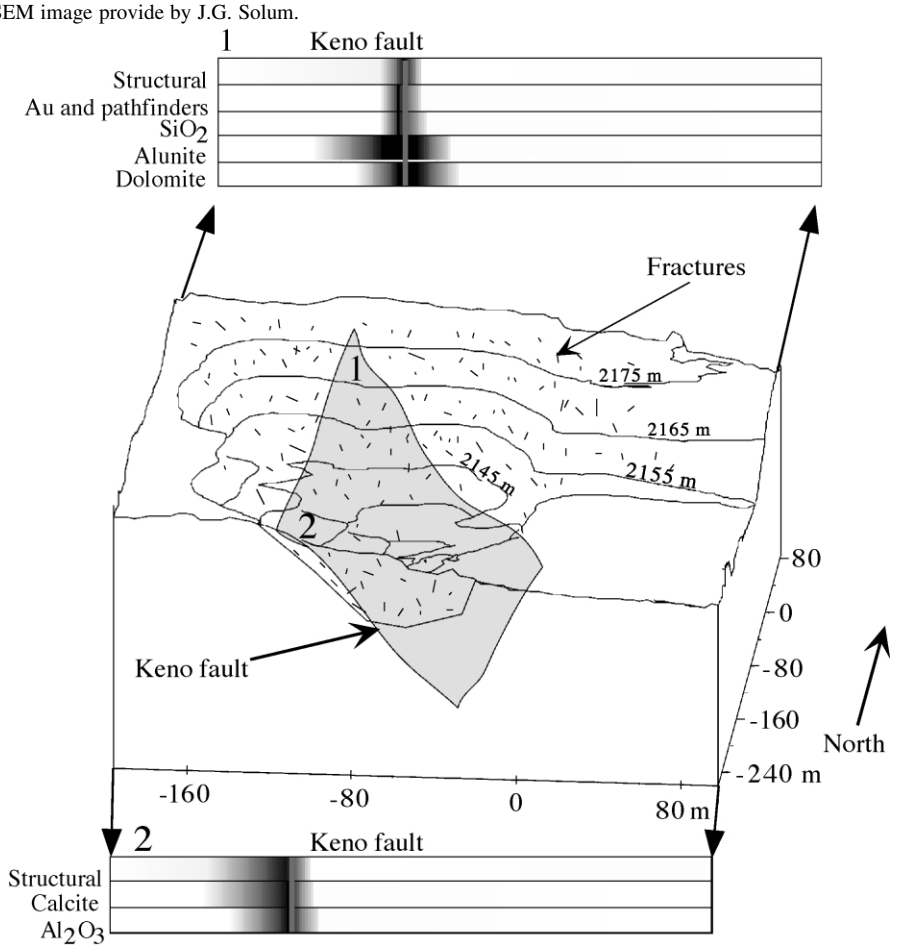

Fig. 15. Keno fault zone structural and geochemical indicators. The widths of the fault zone vary depending on the indicator. The fault can be mapped by offset marker beds and the presence of slickenlines, elemental signatures, and the presence of fault-related minerals (alunite, calcite, dolomite). The maximum width of the fault at both ends of the pit is approximately 20 m.

of gold, interact with faults and fractures to allow ore-bearing fluids to diffuse throughout the rock mass.

We suggest that the Keno fault zone and the fractures associated with it interacted with the pre-existing fracture systems to produce a linear belt of high permeability at the deposit scale. Lack of fracture density correlations with Au content may be due to the length and time scales of fluid flow and chemical reactions that occurred in the system. The faults and fractures may have prepared the rocks for the influx of hydrothermal fluids, but that the total size and detailed distribution of the ore within the deposit were also a function of the volume of hydrothermal fluids available as well as the reactions that occurred within the system.

6. Conclusions

The Keno fault is a moderately sized normal fault that cuts siltstones and silty limestones exposed in an open-pit mine in north central Nevada. It bisects a disseminated-Au deposit and was likely the conduit for ore-bearing fluids. The structural analysis presented here suggests that although fractures are prevalent, no distinct damage zone, as defined by spatial association, exists near the Keno fault zone. The model paragenesis for sedimentary-hosted disseminated gold deposits consists of early, high-temperature deposition of Au, in the form of Au-bearing pyrite, followed by silicification and decarbonization and the development of kaolinite. The presence of early-stage fluid-flow indicators (Au, As, Sb, SiO_2) in the hanging wall and footwall of the fault, and late-stage flow indicators calcite ± barite ± hydrocarbons and the low bulk rock permeability of the Pilot Shale suggest that fractures provided a means for fluids to spread laterally from the fault into the Pilot Shale. The fracturing associated with faulting linked with the pre-existing fractures to provide an interconnected system that was exploited by the Au-bearing fluids.

We show that fault-zone character may change dramatically over short, deposit- or reservoir-scale distances; fault structure, fracture density, and mineralization all vary over the 350-m trace length examined here. We show that while complex, such detailed analyses that combine structural analysis and geochemical data can reveal details of fault zone processes and ore deposition.

Acknowledgments

This study was funded by Enterprise Oil, a Society of Economic Geologists McKinstry Grant, and a Geological Society of America student research grant. We are indebted to Placer Dome U.S. Inc. geologists Jim Brady, Kerry Hart, and Bill Stout, and former Placer Dome U.S. Inc. geologist Jeff Peterson for their insights into the regional geology. Discussion with Connie Nutt about the regional tectonic setting was extremely helpful. John Greg Solum, Matt Pachell, Shanan Peters, and Matt Gallegos assisted with the field studies, and we thank J.G. Solum for sharing some of his unpublished work. Susanne Janecke and Don Fiesinger reviewed this paper and provided insightful comments. Journal reviewers Jonathan Dilles and Fred Chester, and editorial comments by T. Blenkinsop, helped improve the manuscript considerably.

References

Arehart, G.B., 1996. Characteristics and origin of sediment-hosted dissemenated gold deposits: a review. Ore Geology Reviews 11, 383–403.

Armstrong, R.L., 1968. Sevier orogenic belt in Nevada and Utah. Geological Society of America Bulletin 79, 429–458.

Bagby, W.C., Berger, B.R., 1985. Geologic characteristics of sediment-hosted, disseminated precious metal deposits in the western United States. Reviews in Economic Geology 2, 169–202.

Bruhn, R.L., Parry, W.T., Yonkee, W.A., Thompson, T., 1994. Fracturing and hydrothermal alteration in normal fault zones. Pure and Applied Geophysics 142, 609–644.

Caine, J.S., Forster, C.B., 1999. Fault zone architecture and fluid flow: insights from field data and numerical modeling. In: Haneberg, W.C., Mozley, P.S., Moore, J.C., Goodwin, L.B. (Eds.), Faults and Subsurface Fluid Flow in the Shallow Crust. American Geophysical Union Geophysical Monograph 113, pp. 101–127.

Caine, J.S., Evans, J.P., Forster, C.B., 1996. Fault zone architecture and permeability structure. Geology 24, 1025–1028.

Chester, F.M., Logan, J.M., 1986. Implications for mechanical properties of brittle faults from observations of the Punchbowl fault zone, California. Pure and Applied Geophysics 124, 79–106.

Chester, F.M., Evans, J.P., Biegel, R.L., 1993. Internal structure and weakening mechanisms of the San Andreas fault. Journal of Geophysical Research 98, 771–786.

Christensen, O.D., 1995. The Carlin trend giant gold camp: is it the strata, the structure, or the stocks? In: Clark, A.H. (Ed.), Giant Ore Deposits II, Controls on the Scale of Orogenic Magmatic–Hydrothermal Mineralization, Proceedings of the 2nd Giant Ore Deposit Workshop, Queens University, Kingston, Ontario, pp. 402–415.

Coats, R.R., 1987. Geology of Elko County, Nevada. Nevada Bureau of Mines and Geology Bulletin 101.

Committee on Fracture Characterization and Fluid Flow, 1996. Rock Fractures and Fluid Flow: Contemporary Understanding and Applications, National Academy Press, Washington, DC.

Escuder Viruete, J.E., Carbonell, R., Jurado, M.J., Martí, D., Pérez-Estraún, A., 2001. Two-dimensional geostatistical modeling and prediction of the fracture system in the Albala Granitic Pluton, SW Iberian Massif, Spain. Journal of Structural Geology, 23, 2011–2023.

Evans, J.P., Forster, C.B., Goddard, J.V., 1997. Permeability of fault-related rocks, and implications for hydraulic structure of fault zones. Journal of Structural Geology 19, 1393–1404.

Forster, C.B., Zhao, Y., Caine, J.S., Deo, M.D., Nielson, D.L., Kim, J., Cladouhos, T., Bannan, S.A., Snyder, W., Schulz, S.E., Hestir, K., Evans, J.P., 1999. Using an outcrop analog of a shaly reservoir to evaluate the impact of fault-related fracturing on oil production [abs.]. American Association of Petroleum Geologists 1999 annual meeting, A43.

Gillespie, P.A., Howard, C.B., Walsh, J.J., Watterson, J., 1993. Measurement and characterisation of spatial distributions of fractures. Tectonophysics 226, 113–141.

Gutschick, R.C., Rodriguez, J., 1979. Biostratigraphy of the Pilot Shale (Devonian–Mississippian) and contemporaneous strata in Utah,

Nevada and Montana. Brigham Young University Geology Studies 26, 37–63.

Hammond, K.J., 2001. Structural and geochemical analyses of disseminated-gold deposits, Bald Mountain–Alligator Ridge District, Nevada: insights into fault-zone architecture and its effect on mineralization. M.S. Thesis, Utah State University, Logan, 144pp.

Hanks, C.L., Lorenz, J., Teufel, L., Krumhardt, A.P., 1997. Lithologic and structural controls on natural fracture distribution and behavior within the Lisburne Group, northeastern Brooks Range and North Slope subsurface, Alaska. AAPG Bulletin 81, 1700–1720.

Heynekamp, M.R., Goodwin, L.B., Mozley, P.S., Haneberg, W.C., 1999. Controls on fault-zone architecture in poorly lithified sediments, Rio Grande Rift, New Mexico: implications for fault-zone permeability and fluid flow. In: Haneberg, W.C., Mozley, P.S., Moore, J.C., Goodwin, L.B. (Eds.), Faults and Subsurface Fluid Flow in the Shallow Crust, AGU Monograph 113, pp. 27–48.

Hitchborn, A.D., Arbonies, D.G., Peters, S.G., Conners, K.A., Noble, D.C., Larson, L.T., Beebe, J.S., McKee, E.H., 1996. Geology and gold deposits of the Bald Mountain mining district, White Pine County, Nevada. In: Coyner, A.R., Fahey, P.L. (Eds.), Geology and Ore Deposits of the American Cordillera, Geological Society of Nevada, Proceedings, Reno, pp. 505–546.

Hofstra, A.H., Cline, J.S., 2000. Characteristics and models for Carlin-type gold deposits. Society of Economic Geology Reviews 13, 163–220.

Hose, R.K., Blake, M.C. Jr, Smith, R.M., 1976. Geology and mineral resources of White Pine County, Nevada. Nevada Bureau of Mines and Geology Bulletin 85.

Hudec, M.R., 1992. Mesozoic structural and metamorphic history of the central Ruby Mountains metamorphic core complex, Nevada. Geological Society of America Bulletin 104, 1086–1100.

Hulen, J.B., Collister, J.W., 1999. The oil-bearing, Carlin-type gold deposits of Yankee basin, Alligator Ridge district, Nevada. Economic Geology 94, 1029–1050.

Hulen, J.B., Pinnell, M.L., Nielson, D.L., Cox, J.W., Blake, J., 1994. The Yankee mine oil occurrence, Alligator Ridge district, Nevada—an exhumed and oxidized, paleogeothermal oil reservoir. In: Schalla, R.A., Johnson, E.H. (Eds.), Oil Fields of the Great Basin, Nevada Petroleum Society, Reno, pp. 131–142.

Ilchik, R.P., 1990. Geology and geochemistry of the Vantage gold deposits, Alligator Ridge–Bald Mountain mining district, Nevada. Economic Geology 85, 50–75.

Ilchik, R.P., Brimhall, G.H., Schull, H.W., 1986. Hydrothermal maturation of indigenous organic matter at the Alligator Ridge gold deposits, Nevada. Economic Geology 81, 113–130.

Jones, M.E., Huspeni, J.R., 1991. Post gold deposit. In: Buffa, R.H., Coyner, A.R. (Eds.), Geology and Ore Deposits of the Great Basin Field Trip Guidebook Compendium, vol. 1. Geological Society of Nevada, Reno, pp. 865–866.

Klessig, P.J., 1984. History and geology of the Alligator Ridge gold mine, White Pine County, Nevada. In: Johnson, J.L., (Ed.), Exploration for Ore Deposits of the North American Cordillera Field Trip Guidebook, Association of Exploration Geochemists, Reno, pp. 27–35.

Kuehn, C.A., Rose, A.W., 1992. Geology and geochemistry of wallrock alteration at the Carlin gold deposit, Nevada. Economic Geology 87, 1697–1721.

La Pointe, P.R., Hudson, J.A., 1985. Characterization and interpretation of rock mass joint patterns. Geological Society of America Special Paper 1999.

Madrid, R.J., Roberts, R.J., 1991. Origin of gold belts in north central nevada. In: Buffa, R.H., Coyner, A.R. (Eds.), Geology and Ore Deposits of the Great Basin, Geological Society of Nevada, Reno, pp. 927–939.

Mollema, P.N., Antonellini, M., 1999. Development of strike-slip faults in the dolomites of the Sella Group, northern Italy. Journal of Structural Geology 21, 273–292.

Morewood, N.C., Roberts, G.P., 2000. The geometry, kinematics and rates of deformation within an en échelon normal fault segment boundary, central Italy. Journal of Structural Geology 22, 1027–1047.

Morrow, C.A., Shi, L.Q., Byerlee, J.D., 1984. Permeability of fault gouge under confining pressure and shear stress. Journal of Geophysical Research B89, 3193–3200.

Mueller, K.J., Snoke, A.W., 1993. Progressive overprinting of normal fault systems and their role in Tertiary exhumation of the East Humboldt–Wood Hills metamorphic complex northeast Nevada. Tectonics 12, 361–371.

Nolan, T.B., Merriam, C.W., Williams, J.S., 1956. The stratigraphic section in the vicinity of Eureka, Nevada. U.S. Geological Survey Professional Paper 276.

Nutt, C.J., 1996. Cretaceous(?) to early Oligocene sedimentary and volcanic rocks at Alligator Ridge, Buck Mountain–Bald Mountain area, central Nevada. In: Taylor, W.J., Langrock, H. (Eds.), Cenozoic Structure and Stratigraphy in Central Nevada, Field Conference Volume, Nevada Petroleum Society, Reno, pp. 13–18.

Nutt, C.J., 1997. Sequence of deformational events and the recognition of Eocene(?) deformation in the Alligator Ridge area, east-central Nevada. Society of Economic Geologists Guidebook Series 28, 203–211.

Nutt, C.J., Good, S.C., 1998. Recognition and significance of Eocene deformation in the Alligator Ridge area, central Nevada. In: Tosdal, R.M. (Ed.), Contributions to the Gold Metallogeny of Northern Nevada. U.S. Geological Survey Open File Report 98-338, pp. 141–150.

Nutt, C.J., Hofstra, A.H., Hart, K.S., Mortensen, J.K., 2000. Structural setting and genesis of gold deposits in the Bald Mountain–Alligator Ridge area, east-central Nevada. In: Cluer, J.K., Price, J.G., Struhsacker, E.M., Hardyman, R.F., Morris, C.L. (Eds.), Geology and Ore Deposits 2000: The Great Basin and Beyond, Geological Society of Nevada, Proceedings, Reno, pp. 513–537.

Pancoast, L.E., 1986. Geology of the east flank of Alligator Ridge, White Pine County, Nevada. M.S. thesis, University of Idaho.

Pinnell, M.L., Blake, J.G., Hulen, J.B., 1991. Active oil seep at Nevada gold mine holds intrigue for more exploration. Oil and Gas Journal 89, 74–79.

Rawling, G.C., Goodwin, L.B., Wilson, J.L., 2001. Internal architecture, permeability structure, and hydrologic significance of contrasting fault-zone types. Geology 29, 43–46.

Roberts, R.J., Ferguson, H.G., Gilluly, J., Hotz, P.E., 1958. Paleozoic rocks of north-central Nevada. American Association of Petroleum Geologists Bulletin 42, 2813–2857.

Rota, J.C., 1993. Geology and related studies at the Gold Quarry deposit, Nevada. In: Christensen, O.D. (Ed.), Gold Deposits of the Carlin Trend, Nevada. Society of Economic Geologists Guidebook Series 18, pp. 67–78.

Schulz, S.E., Evans, J.P., 1998. Spatial variability in microscopic deformation and composition of the Punchbowl fault, southern California: implications for mechanisms, fluid-rock interaction, and fault morphology. Tectonophysics 295, 223–244.

Schulz, S.E., Forster, C.B., Evans, J.P., Nielson, D.L., Hestir, K., 1998. Characterizing and modeling fractures and faults in an exhumed petroleum reservoir [abs.]. American Association of Petroleum Geologists 1998 annual meeting, A99.

Seront, B., Teng-Fong, W., Caine, J.S., Forster, C.B., Bruhn, R.L., Fredrich, J.T., 1998. Laboratory characterization of hydromechanical properties of a seismogenic normal fault system. Journal of Structural Geology 20, 865–881.

Sibson, R.H., Scott, J., 1998. Stress/fault controls on the containment and release of overpressured fluids: examples from gold-quartz vein systems in Juneau, Alaska; Victoria, Australia and Otago, New Zealand. Ore Geology Reviews 13, 293–306.

Sigda, J.M., Goodwin, L.B., Mozley, P.S., Wilson, J.L., 1999. Permeability alteration in small-displacement faults in poorly lithified sediments: Rio Grande Rift, central New Mexico. In: Haneberg, W.C., Mozley, P.S., Moore, J.C., Goodwin, L.B. (Eds.), Faults and Subsurface Fluid Flow in the Shallow Crust, AGU Monograph 113, pp. 51–68.

Smith, L., Forster, C.B., Evans, J.P., 1990. Interaction of fault zones, fluid flow, and heat transfer at the basin scale. In: Neuman, S.P., Neretnieks,

I. (Eds.), Hydrogeology of Low Permeability Environments, Hydrogeology Selected Papers 2, Verlag Heinz Heis, Hanover, pp. 41–67.

Snoke, A.W., Howard, K.A., McGrew, A.J., Burton, B.R., Barnes, C.G., Peters, M.T., Wright, J.E., 1997. The grand tour of the Ruby–East Humboldt metamorphic core complex, northeastern Nevada. Part 1—introduction and road log. Brigham Young University Geology Studies 42, 225–269.

Stenger, D.P., Kesler, S.E., Peltonen, D.R., Tapper, C.J., 1998. Deposition of gold in carlin-type deposits: the role of sulfidation and decarbonation at Twin Creeks, Nevada. Economic Geology 93, 201–215.

Stewart, J.H., 1972. Initial deposits in the Cordilleran geosyncline; evidence of a Late Precambrian (<850 Ma) continental separation. Geological Society of America Bulletin 83, 1345–1360.

Stout, B., 1996. Geologic overview of the Yankee mine, White Pine County, Nevada. In: Jones, E.A. (Ed.), Geology and Gold Deposits of Eastern Nevada. Geological Society of Nevada, 1996 Spring Fieldtrip Guidebook, Special Publication 23, pp. 105–110.

Teal, L., Jackson, M., 1997. Geologic overview of the Carlin Trend gold deposits and descriptions of recent deep discoveries. Society of Economic Geologists Guidebook Series 28, 3–37.

Titley, S.R., Thompson, R.C., Haynes, F.M., Manske, S.L., Robison, L.C., White, J.L., 1986. Evolution of fractures and alteration in the Sierrita-Esperanza hydrothermal system, Pima County, Arizona. Economic Geology 81, 343–370.

Volk, J.A., Lauha, E., Leonardson, R.W., Rahn, J.E., 1996. Structural geology of the Betze-Post and Meikle Deposits, Elko and Eureka Counties, Nevada. In: Green, S.M., Struhsacker, E. (Eds.), Ore Deposits of the America Cordillera Field Trip Guidebook Compendium, Geological Society of Nevada, Reno, pp. 180–194.

Williams, C.L., Thompson, T.B., Powell, J.L., Dunbar, W.W., 2000. Gold-bearing breccias of the Rain Mine, Carlin trend, Nevada. Economic Geology 95, 391–404.

Yielding, G., Freeman, B., Needham, D.T., 1997. Quantitative fault seal prediction. American Association of Petroleum Geologists Bulletin 81, 897–917.